FGGE Reanalysis at GFDL

J. J. PLOSHAY, W. F. STERN, AND K. MIYAKODA

Geophysical Fluid Dynamics Laboratory/NOAA, Princeton University, Princeton, New Jersey

(Manuscript received 4 September 1991, in final form 11 December 1991)

ABSTRACT

The reanalysis of FGGE [First GARP (Global Atmospheric Research Program) Global Experiment] data for 128 days during two special observing periods has been performed, using an improved data-assimilation system and the revised FGGE level II dataset. The data-assimilation scheme features forward continuous (in time) data injection in both the original and the new systems. However, the major revisions in the new system include a better first guess and a more efficient dynamical balancing for the assimilation of observed data. The results of the implementation of this system are assessed by intercomparisons among the new FGGE analysis of other institutions such as ECMWF (European Centre for Medium-Range Weather Forecasts) and NMC (National Meteorological Center, Washington, D.C.), and also the original GFDL (Geophysical Fluid Dynamics Laboratory) analysis. The quality of the new GFDL analysis is now comparable to those of the other two institutions. However, the moisture analysis appears to be appreciably different, suggesting that the cumulus convection parameterizations and the boundary-layer moisture fluxes in the models are responsible for this discrepancy.

A detailed investigation of the results has been carried out by comparing the analyses with radiosonde observations. This verification reveals that temperature and wind differences have been reduced considerably from the original to the new GFDL analysis; they are now competitive with those of ECMWF and NMC, while with regard to the geopotential height, differences of the GFDL reanalysis are larger than the original GFDL as well as the ECMWF and the NMC. A comparative study is also made with UCLA analyses over Asia in connection with the Indian monsoon. The results indicate that the qualities of both analyses are comparable. The capability of representing Madden–Julian oscillations in the reanalysis and in the ECMWF and old GFDL analysis is investigated by comparing with satellite observations. It is revealed that these oscillations are successfully reproduced by the new analysis; however, the agreement with the satellite data is not quite satisfactory. The utilization of satellite-observed wind (satobs) and aircraft data (aireps) in the data assimilation needs particular care. It appears that the quality control of these data in the GFDL reanalysis is too restrictive; in other words, the toss-out criterion of wind data is too small. A consequence of the failure to accept some single-level data turns out to be a fairly large discrepancy in representing the maximum wind speed in the analysis. It is also discussed that the current forward continuous-injection scheme is not adequate to obtain diabatic quantities for the archive.

1. Introduction

One of the primary objectives of FGGE [First GARP (Global Atmospheric Research Program) Global Experiment] was to evaluate data-assimilation systems by applying them to a diverse set of global observations. GFDL (Geophysical Fluid Dynamics Laboratory) has been a participant in this international activity from the beginning, and in 1982 applied the continuous data-injection method to the so-called level IIb dataset taken during 1979, resulting in a benchmark level IIIb dataset.

The original analysis results were documented in four volumes (Ploshay et al. 1983), and archived at the World Data Center, Asheville, North Carolina. Comments on the analyses were given by Miyakoda et al. (1983) and Miyakoda (1985). Lau (1984a,b) produced circulation statistics and a comparison of two sets of analyses, the original GFDL and the original ECMWF (European Centre for Medium-Range Weather Forecasts) analyses, the ECMWF being another major participant in the original FGGE analysis production (Bengtsson et al. 1982). Overall deficiencies of these analyses were noted as follows: GFDL analyses were noisier than the ECMWF analyses, and also showed a tendency to produce a shallower representation of some intense cyclones (Stern et al. 1985). Another characteristic is that the vertical velocities were stronger in the GFDL analysis than in the ECMWF analysis, especially in the tropics (Kung and Tanaka 1983). Arpe (1984) noted that the ECMWF analysis was more faithful to the available data than the GFDL analysis; the reason for the poor fit to the observations of the latter is attributed to small-scale irregularities in the analyzed patterns.

The data-assimilation system has recently been re-

Corresponding author address: Jeffrey Ploshay, Princeton University, NOAA/ERL/GFDL, Forrestal Campus, US Route 1, P.O. Box 308, Princeton, NJ 08542.

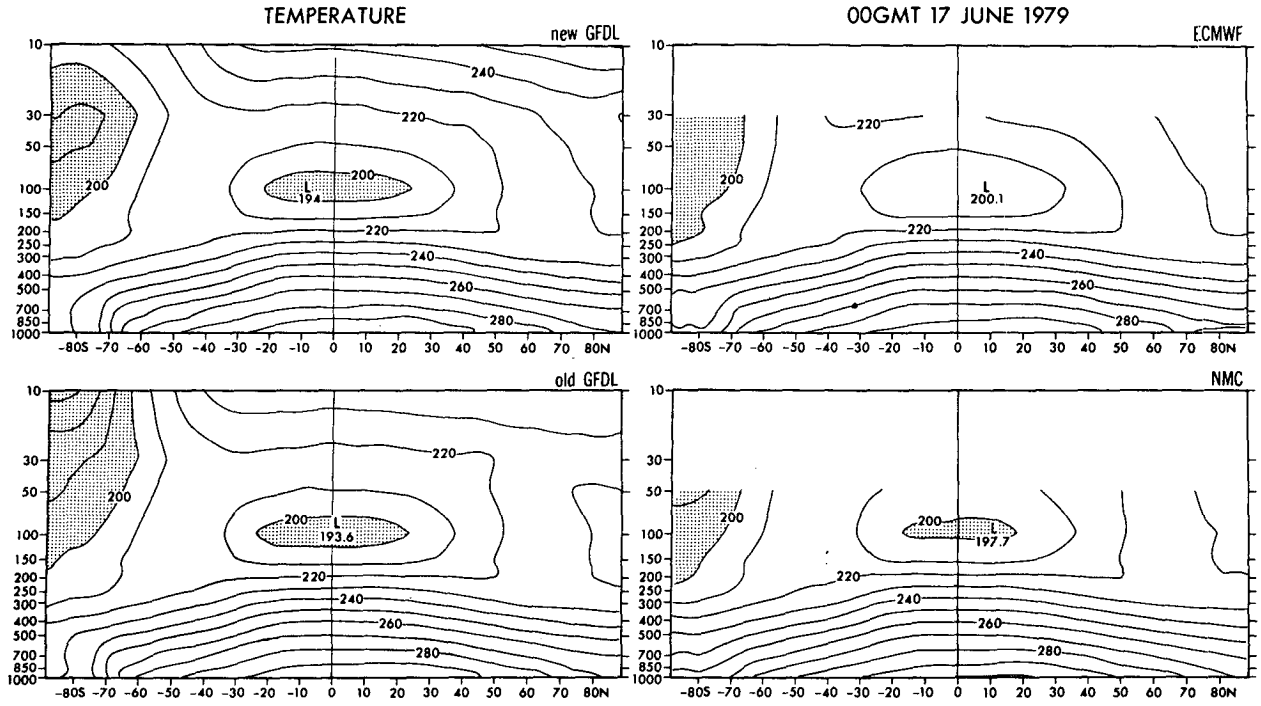

FIG. 1a. Meridional sections for temperature (K). The areas in which the temperature is lower than 200 K are stippled.

vised at GFDL (Stern and Ploshay 1992). In summary, the outstanding features of the revised GFDL system are listed in Table 1. Data assimilation has been carried out by applying this new system to the updated FGGE level IIb dataset and producing a reanalyzed level IIIb dataset. The analysis was performed only for two periods, SOP I (special observing period I, 5 January–10 March 1979) and SOP II (27 April–30 June 1979).

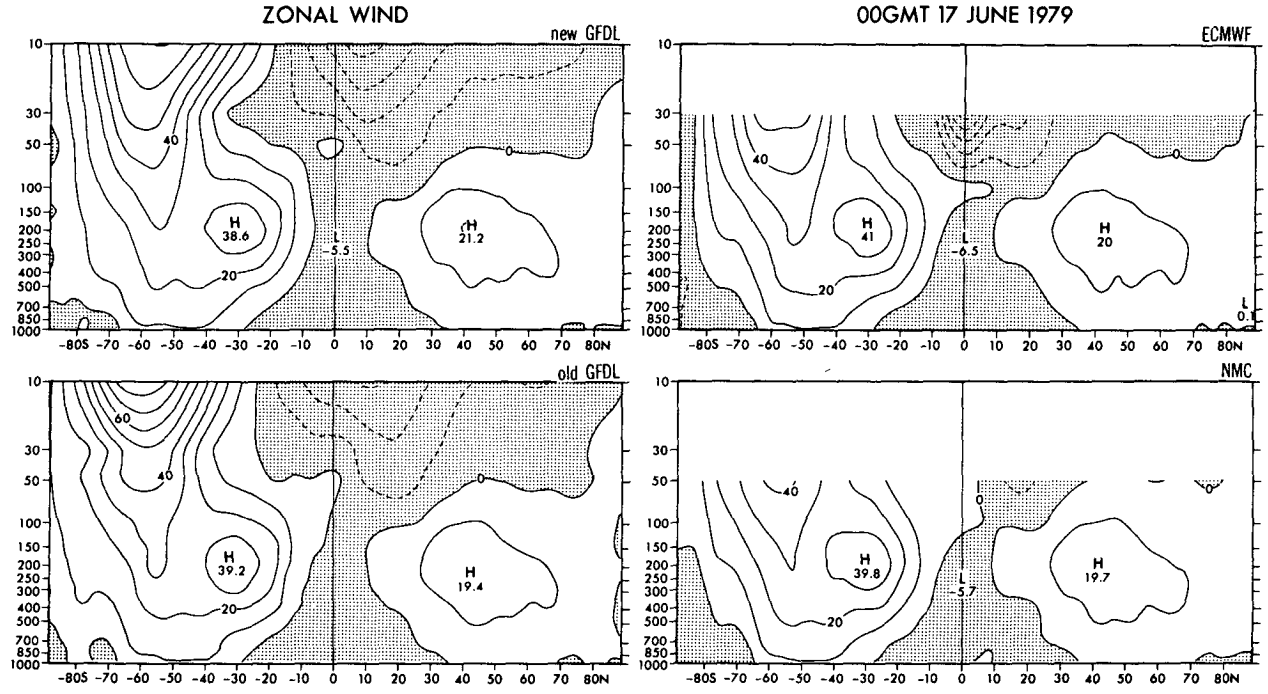

FIG. 1b. The same as Fig. 1a except for zonal wind (m s^{-1}). The negative (easterlies) regions are stippled.

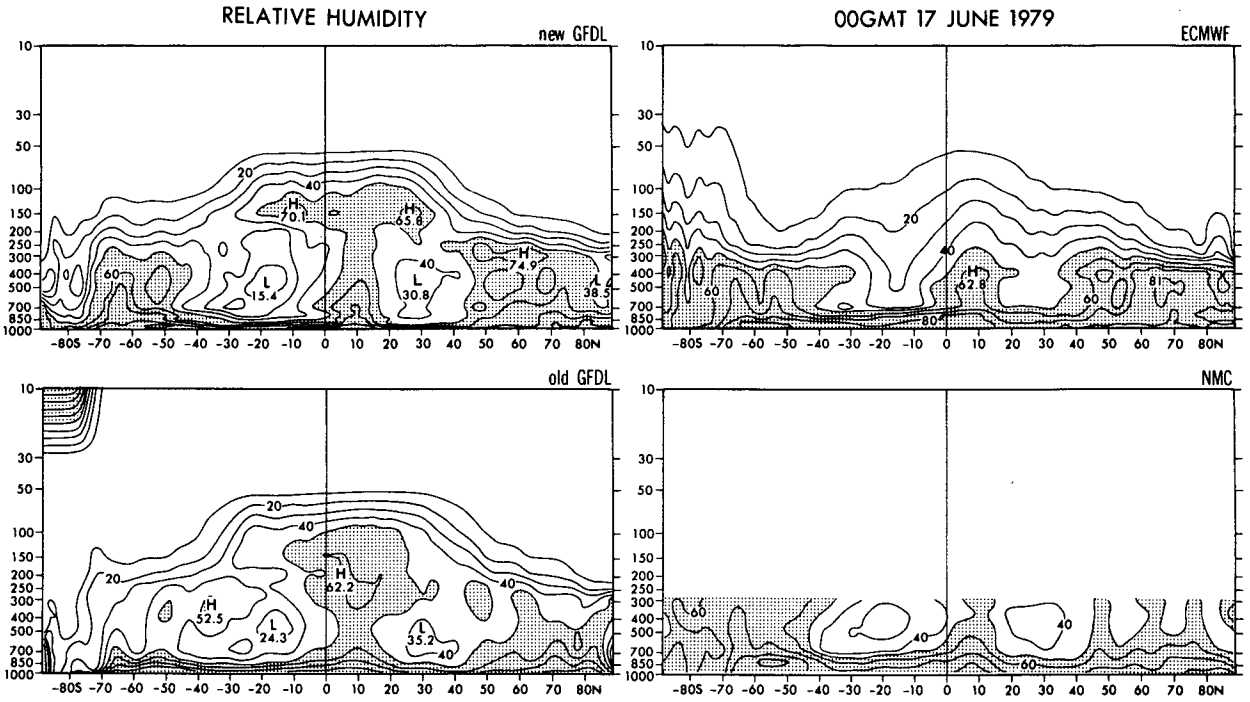

FIG. 1c. The same as Fig. 1a except for relative humidity (%). The areas in which the humidity is higher than 50% are stippled.

Compared with the original FGGE analysis, the new analysis appears to exhibit substantial improvement in its quality.

In general, it is the objective for a data-assimilation system to reach a state where there is a time and spatial consistency among the variables, remaining faithful to the observations, and minimizing constraints that might conflict with the model's internal consistency such as geostrophic balance.

2. Intercomparison of various analyses

a. Four analyses

Comparison is made among four analyses, the GFDL, ECMWF, and NMC (National Meteorological Center, Washington, D.C.) reanalyses and the original GFDL analysis. The current ECMWF and NMC operational data-assimilation systems have been revised since their FGGE reanalyses were produced. Figures 1a–c show the latitude–height cross sections of the zonally averaged variables for 0000 UTC 17 June 1979. The gaps in the stratosphere for the ECMWF and NMC cross sections indicate where their archiving terminated.

TABLE 1. Revision of GFDL's continuous data-assimilation system.

New	Old
First guess from 6-h forecast	First guess from 12-h persistence
500-km data-collection radius	250-km data-collection radius
Incremental linear normal-mode initialization for each time step	Nonlinear normal-mode initialization every 6 h
R42L18 model	R30L18 model
Data insertion at all levels	No data insertion at top two levels

The cross sections of zonal-mean temperature are presented in Fig. 1a. The difference between the two GFDL maps is primarily in the Southern Hemisphere polar stratosphere. Since the original GFDL assimilation did not have data inserted at the top two levels, the winter pole cooled unrealistically (<170 K) in the model's top levels. The GFDL tropical tropopause temperatures are the lowest (194 K); and ECMWF is the warmest (200.1 K) (Lau 1984a), with NMC in between (197.7 K). NMC has the warmest surface temperatures (300-K contour).

The cross section of zonal-mean zonal wind, shown in Fig. 1b, has tropospheric, midlatitude, Northern, and Southern Hemisphere jets that are similar in magnitude and structure. The ECMWF Southern Hemisphere jet is slightly stronger than the others, and the GFDL reanalysis has the strongest Northern Hemisphere jet. ECMWF has a spurious easterly jet at the equator near 30–50 hPa. The original GFDL Southern Hemisphere high-latitude stratospheric jet is too strong due to the spurious temperature gradient.

In the relative humidity cross sections (Fig. 1c),

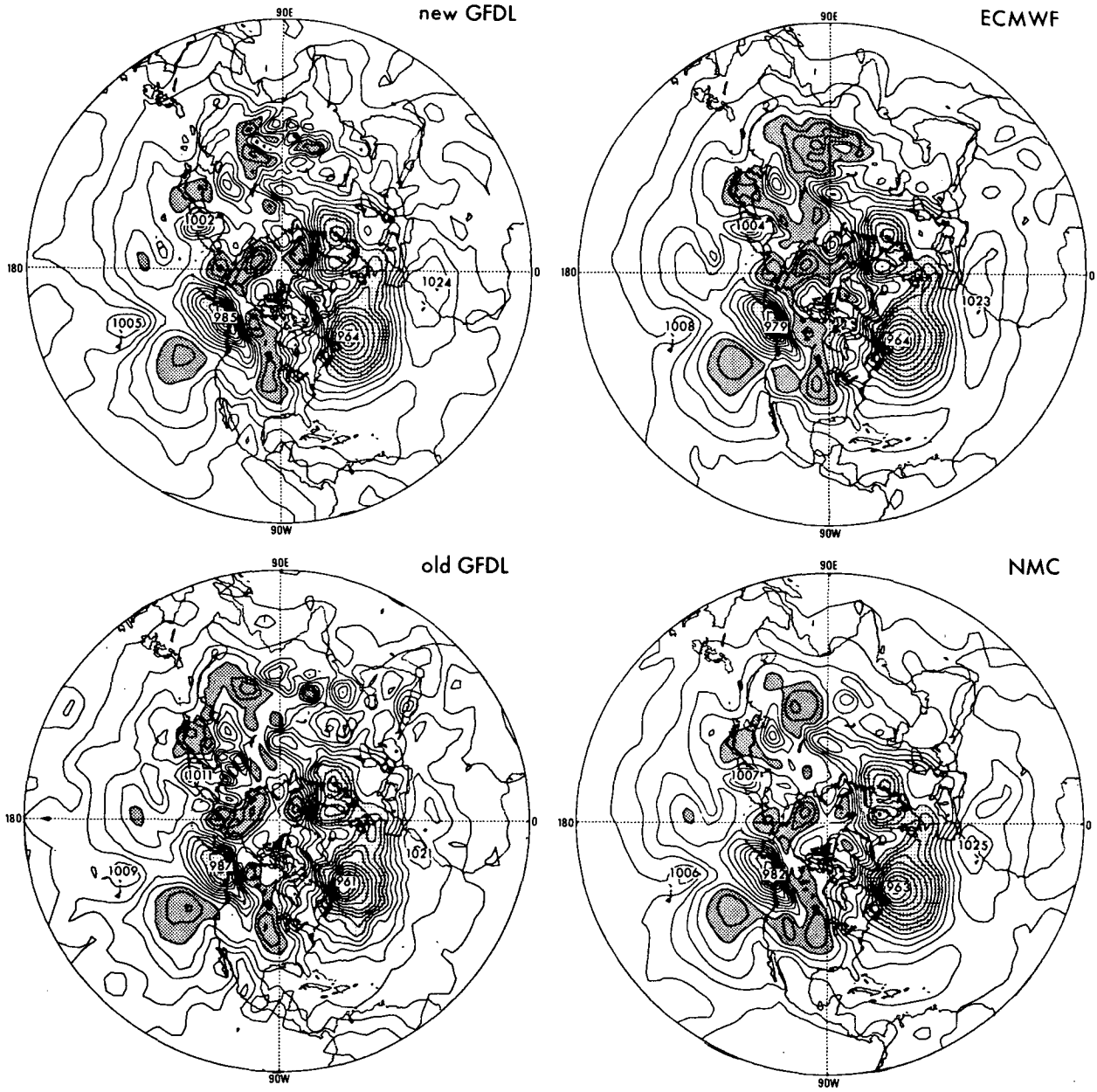

FIG. 2a. Stereographic maps of sea level pressure (hPa). Contour interval is 4 hPa.

NMC archives only up to 300 hPa. Relative humidity is compared due to the fact that moisture observations were in that form. The differences between the analyses are more pronounced, with both GFDL analyses having high values at higher levels in the tropics, while ECMWF has the deepest layer of 80% relative humidity near the tropical and subtropical surface. The GFDL subtropical latitudes are the driest. At higher latitudes, the GFDL reanalysis is more humid than the original GFDL. The moisture in the new GFDL analysis appears to remain closer to the surface than that in the old GFDL, and much more so than in the other analyses. This is due to differences in the treatment of the boundary-layer processes in the models. The ECMWF is most humid in the Northern Hemisphere higher latitudes and the NMC is the most humid in the Southern Hemisphere higher latitudes. The stratospheric Southern Hemisphere relative humidity maximum in the original GFDL is fictitiously generated by temperatures that are too cold. Cumulus convection parameteriza-

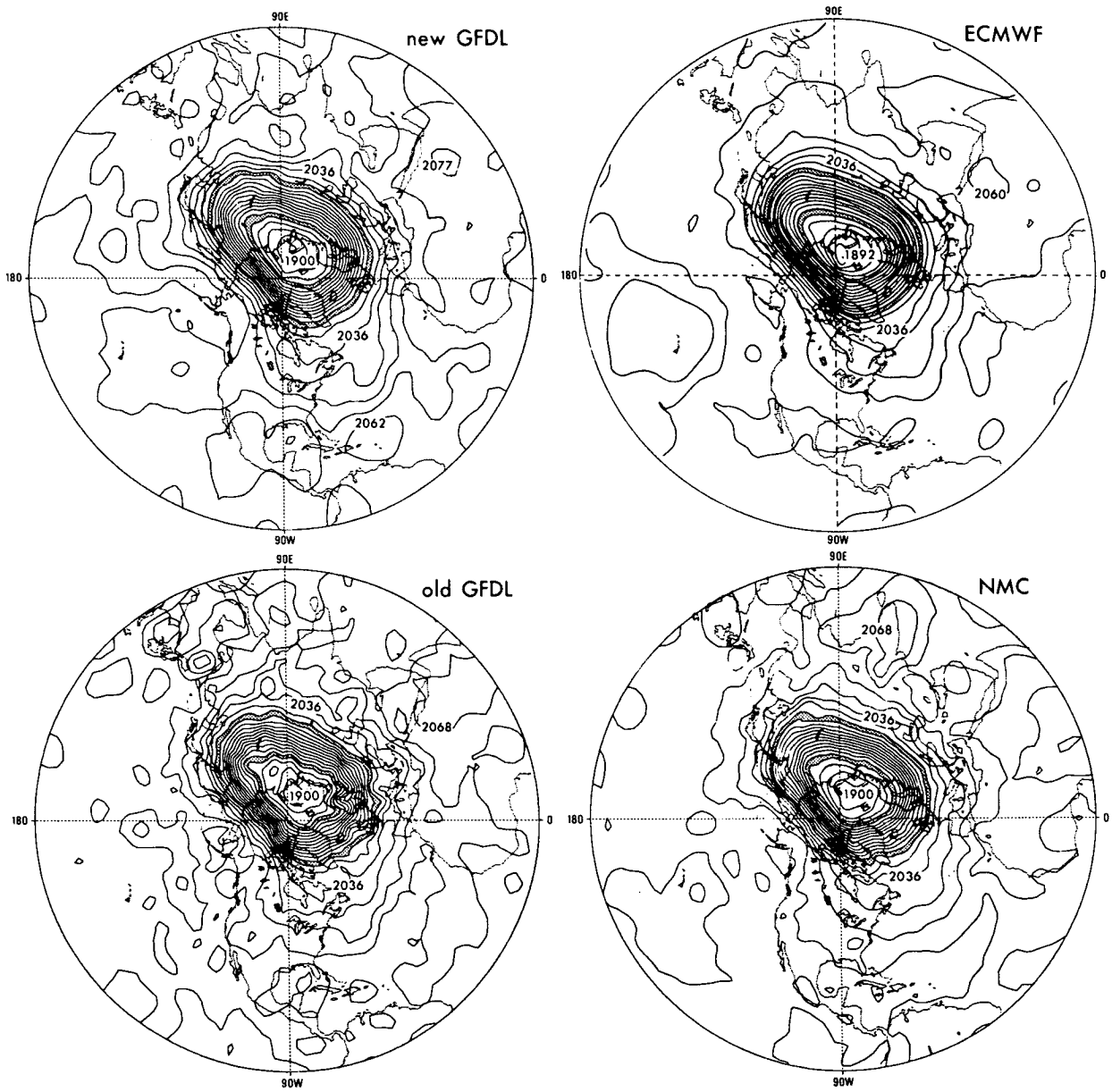

FIG. 2b. Stereographic maps of geopotential height (dam) at 50 hPa. Contour interval is 8 dam.

tion scheme differences together with the humidity saturation value of 100% probably are responsible for much of the relative humidity differences between the centers. GFDL uses moist-convection adjustment, while ECMWF and NMC employ two different Kuo schemes.

To study the characteristics of data-assimilation systems it is useful to look at single-day comparisons. Figures 2a–d show a comparison of the four analyses from a hemispheric point of view for a single day, 0000 UTC 5 February 1979. Sea level pressure (Fig. 2a) shows the reduction in noisiness in the new GFDL, with generally deeper lows compared to the old GFDL, particularly the low northeast of Japan. Upper-level features (Figs. 2b–d) are quite similar in the three reanalyses, excluding the old GFDL, which has small-scale noisiness that tends to result in somewhat shallower features with different phase speeds. Other examples of Southern Hemispheric maps are shown in Ploshay et al. (1991).

Figure 3 depicts the 200-hPa monthly mean zonal winds for January 1979 for the four analyses. The high-speed zones are very similar for the GFDL, ECMWF, and NMC reanalyses with maxima of 69.4, 71.3, and

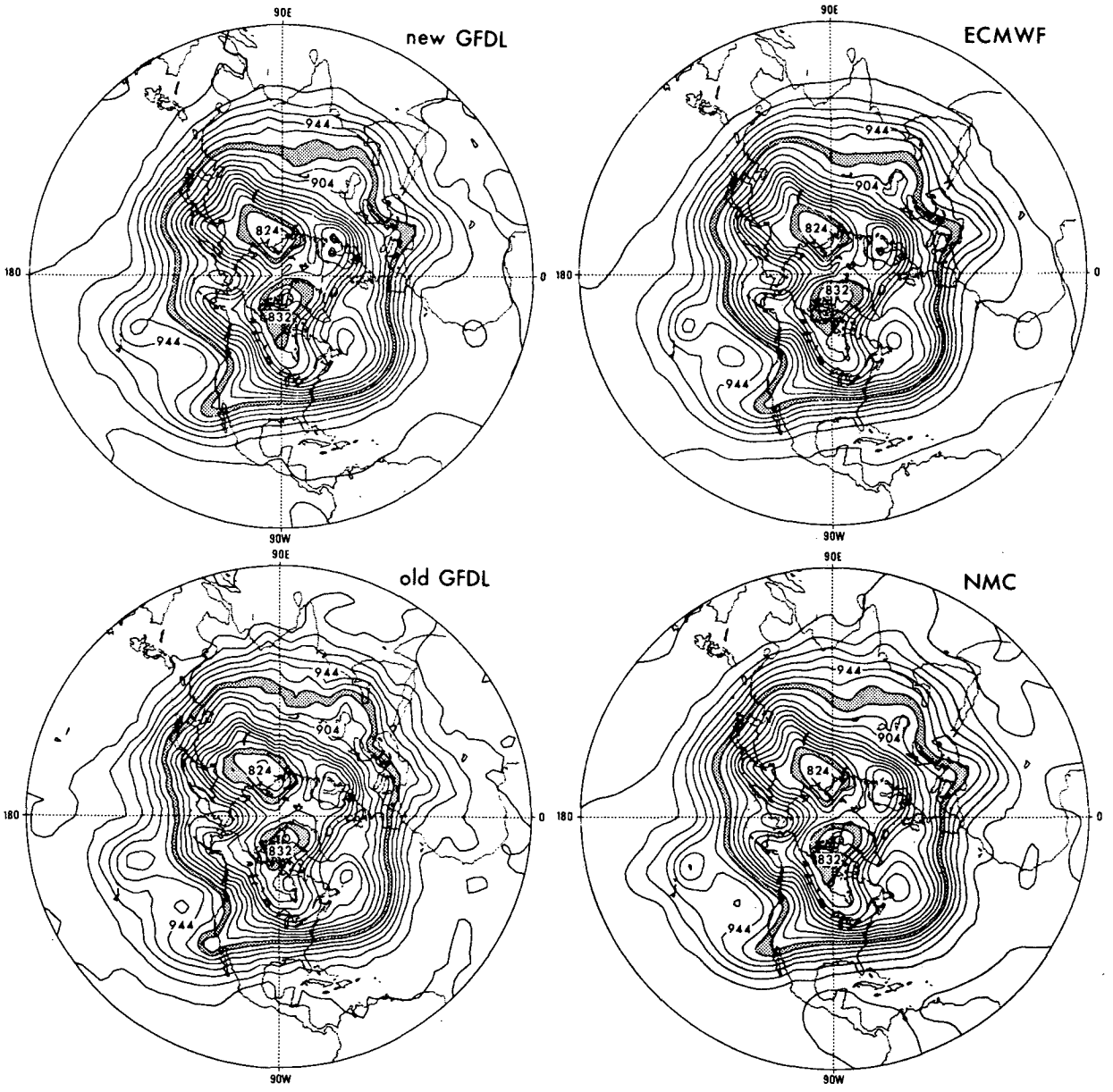

FIG. 2c. 300 hPa Northern Hemisphere. Units are dekameters. Coutour interval is 8 dam.

71.8 m s^{-1}, respectively. The original GFDL analysis has a slightly smaller region of dark stippling with a maximum value of 63.2 m s^{-1}. Feature for feature, the three reanalyses are similar in both magnitude and structure. Noisiness is seen in the original GFDL. The largest differences between the original and the reanalyses appears off the west coast of South America (near 100°W at the equator) where GFDL, ECMWF, and NMC jets are 28.3, 25.7, and 24.8 m s^{-1}, respectively, while the original GFDL is less than 20 m s^{-1}. Another large difference occurs in the South Pacific near 130°W.

b. Previous papers

Hollingsworth et al. (1985) compared results of three operational centers, ECMWF, United Kingdom Meteorological Office (UKMO), and NMC. Their intercomparisons of the original FGGE analyses focused on the sources of some analysis differences and the impact of the analysis differences on forecast quality during five days, 15–19 February 1979. It was shown that, during this period, a crucial quality-control decision in one system led to incorrect baroclinic development in the forecasts. Specifically, the NMC analyses

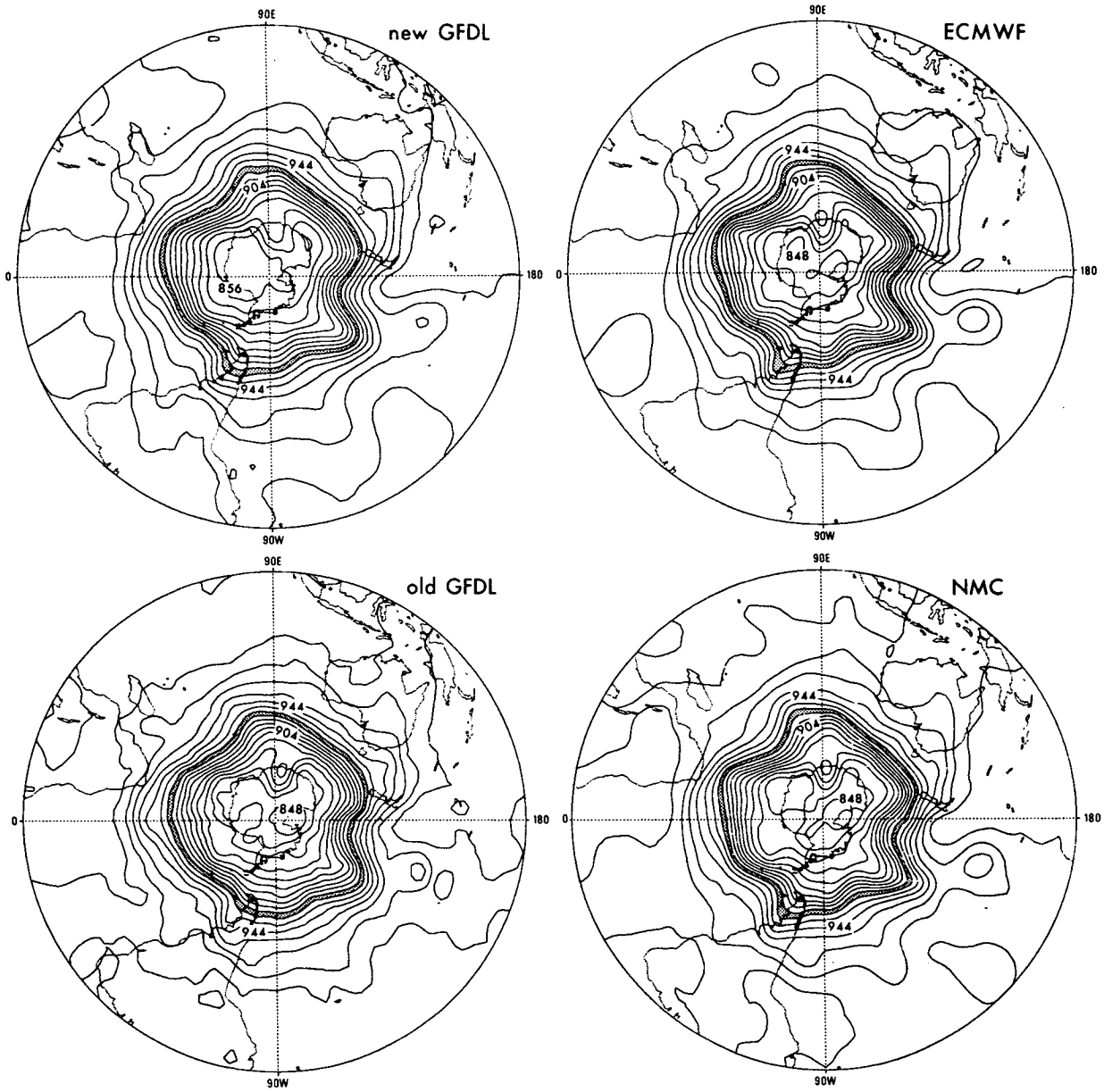

FIG. 2d. 300 hPa Southern Hemisphere. Units are dekameters. Contour interval is 8 dam.

rejected wind reports from aircraft *40614* (see Fig. 16) and nearby cloud winds in the gross-error check due to first-guess errors. The resulting NMC analysis produced a weaker upper-level jet.

The GFDL reanalysis had a similar problem: due to the analysis system's earlier rejection of wind data, the first guess did not forecast a strong enough jet near the date line in the North Pacific at 250 hPa on 17 February, where data from aircraft *40614* and adjacent cloud winds were rejected, while the ECMWF and UKMO accepted them. Interestingly, the ECMWF and original GFDL analyses both have the same jet maximum value of 79.6 m s^{-1}, whereas the GFDL and NMC reanalyses both arrive at a similar analysis. This can be seen in the wind fields at 250 hPa and the cross sections through the date line in Figs. 4 and 5.

Since much of the wind data over oceans is of the single-level type such as satobs and aireps, "analysis over oceans is probably the most difficult and important of all analysis problems, because of the scarcity of data over these enormous regions" (Hollingsworth 1986). See section 5 for an experiment with more lenient wind-data acceptance criterion and the resultant strengthened jet.

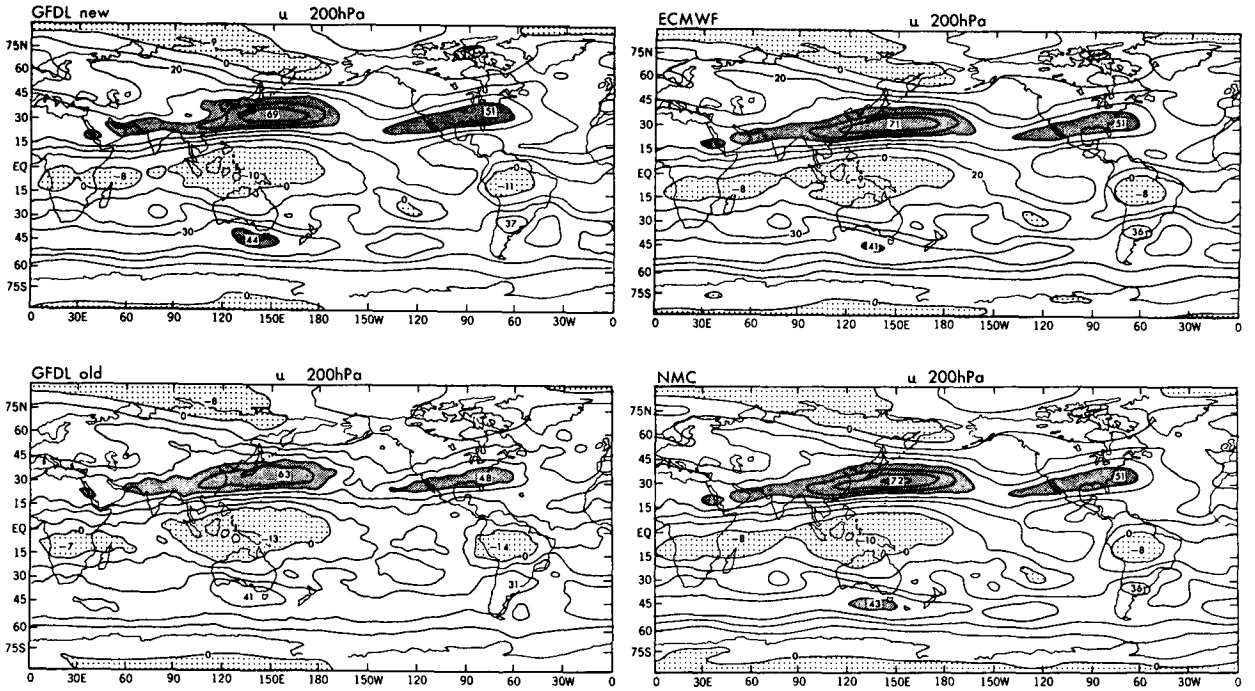

FIG. 3. Isotach maps for the January 1979 monthly mean zonal wind u at 200 hPa. The areas in which wind speeds are greater than 40 m s^{-1} are shaded, while the easterly wind areas are stippled.

c. *UCLA analyses*

He et al. (1987) (hereafter called UCLA) employed a successive correction method, with the "main" ECMWF analysis (Bengtsson et al. 1982) as a first guess, in studying the Tibetan plateau and Indian monsoon regions. They were one of the few groups involved in the analysis of FGGE data and incorpo-

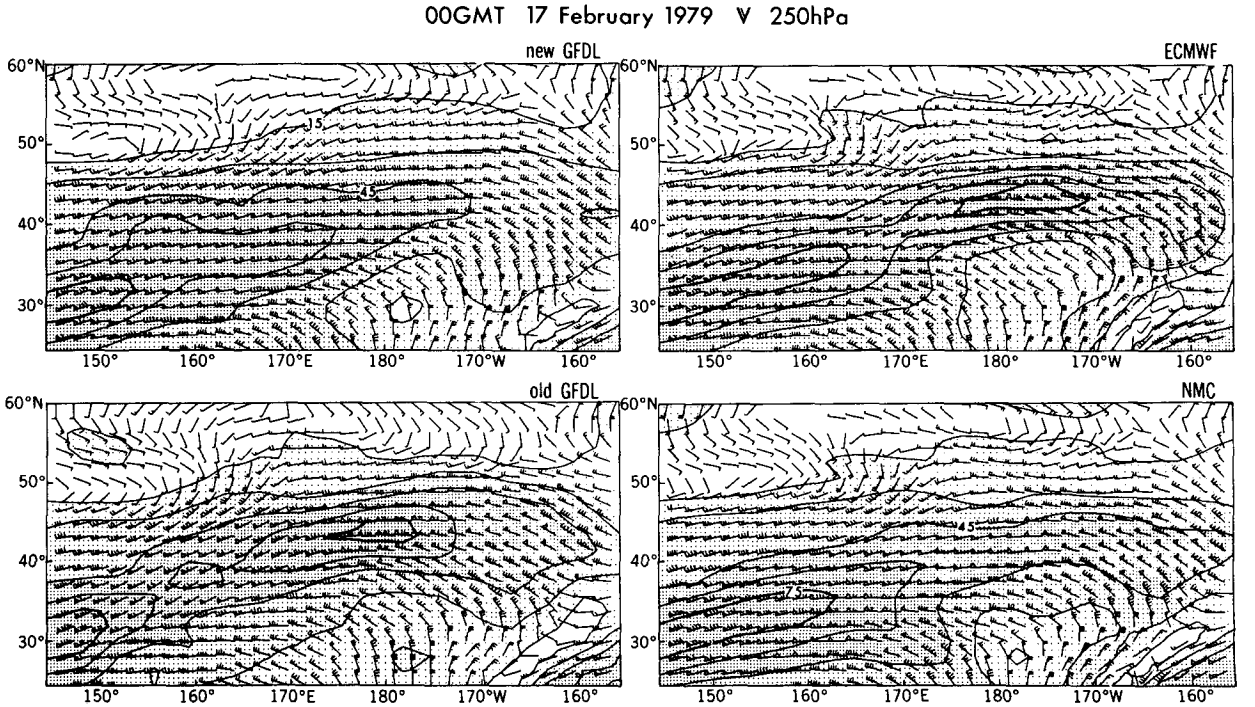

FIG. 4. Wind arrows and isotachs (m s^{-1}), contour interval is 15 m s^{-1}.

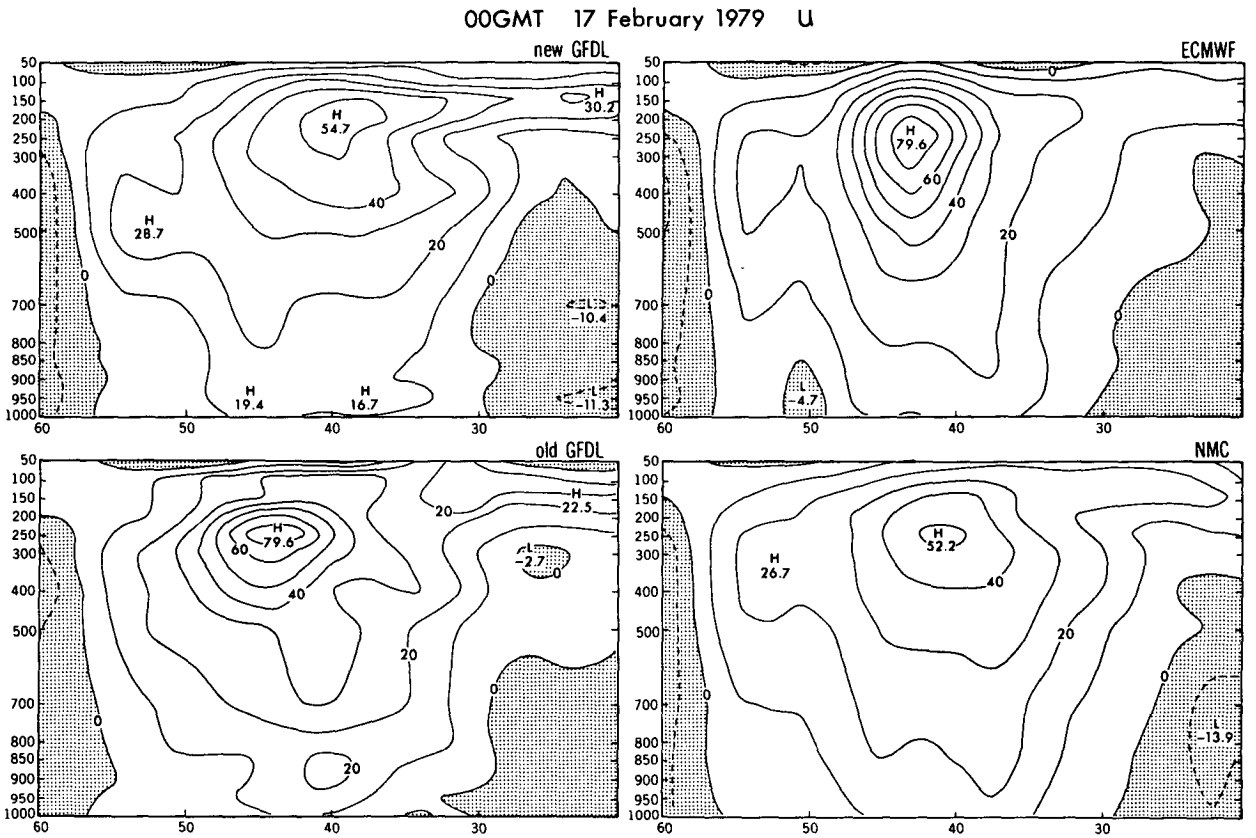

FIG. 5. Latitude–height sections through the date line for the intensity of zonal wind (m s^{-1}). The negative (easterlies) regions are stippled.

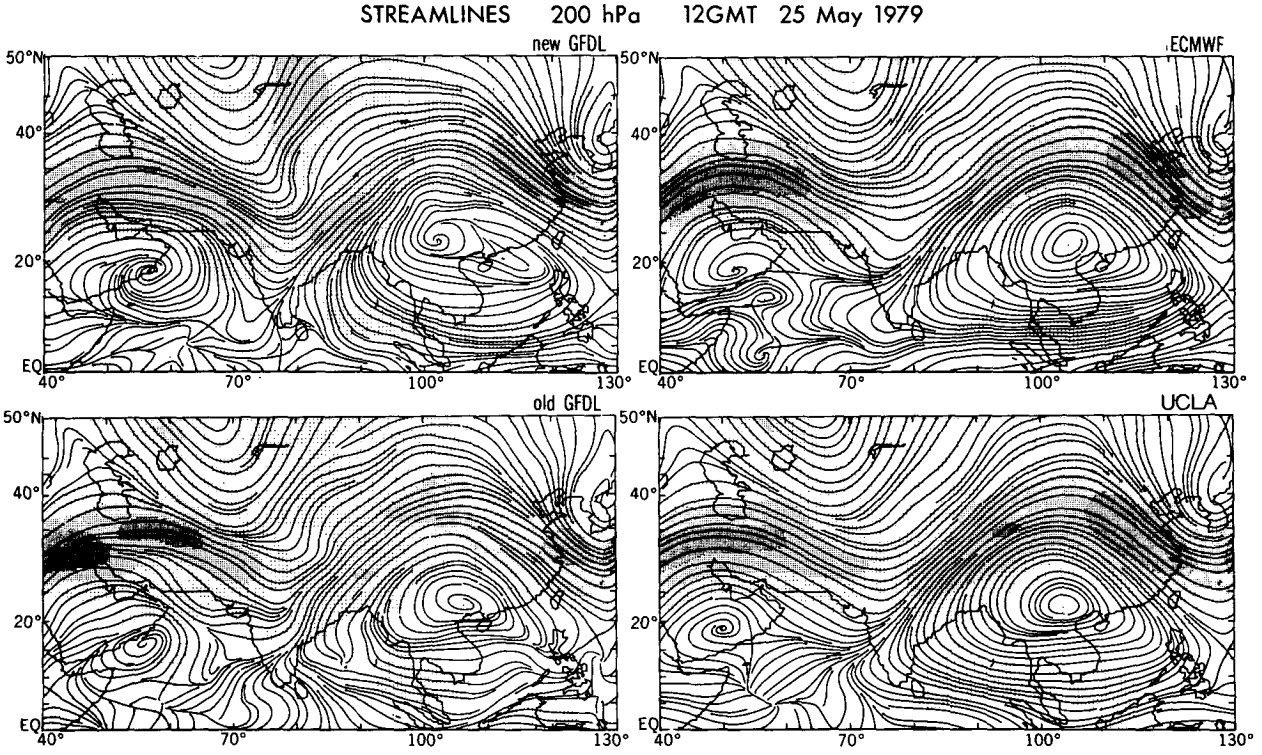

FIG. 6. Streamlines and isotachs centered near India. The isotachs are shown by shading, with a shading intensity interval of 15 m s^{-1}; darkest shading indicates wind intensities of greater than 45 m s^{-1}.

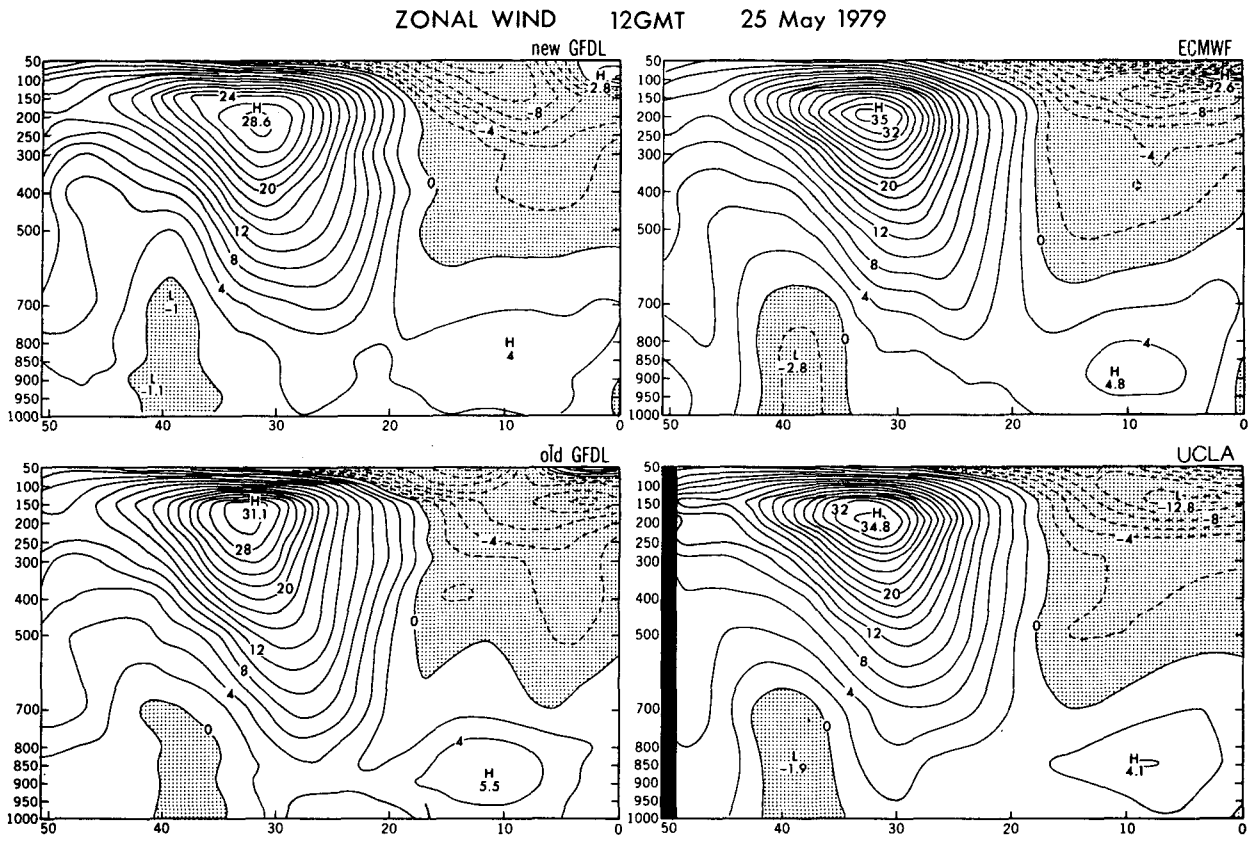

FIG. 7a. Latitude–height sections of zonal winds (m s^{-1}), averaged over the longitudes from 40° to 130°E. The contour interval is 2 m s^{-1}. The negative (easterlies) regions are stippled.

rated special observations from over China using an objective analysis scheme, as opposed to a model data assimilation, in order to obtain a more reliable analysis over and around the Tibetan plateau for heat and moisture budget computations.

Figure 6 shows an example of streamlines and isotachs at 200 hPa at 1200 UTC 25 May 1979, over the region studied by the UCLA group. The four panels are the same format as previous figures, with the NMC reanalysis replaced by the UCLA in the layout.

In Fig. 7a, the zonal-mean zonal wind over the study region (between 40° and 130°E) shows similarity between the ECMWF and UCLA, as one might expect. The GFDL reanalysis has the weakest westerly jet, at 200 hPa, of the four panels; however, the contours coincide quite well at speeds less than 22 m s^{-1}. The lower wind speeds in the GFDL reanalysis are a result, once again, of the first guess underforecasting the jet maximum and sparse single-level cloud winds being rejected. See section 5.

The GFDL reanalysis and UCLA relative humidity cross sections appear to be the most similar in Fig. 7b. For example, the area of greater than 50% relative humidity extends to about 22°N at 100 hPa and to near 500 hPa at the equator, with similar minimums near 400 hPa at 12°N (27.1%, GFDL; 26%, UCLA). UCLA analyzed moisture only up to 200 hPa.

d. Indian monsoon

Following Krishnamurti et al. (1981), a comparison was made of the onset times of the Indian monsoon among the four analyses, that is, new and old GFDL, ECMWF, and NMC. Longitudinal averages of the zonal and meridional winds at 850 hPa were taken over the longitudes from 50° to 70°E, and latitudes from 30°S to 40°N (rectangle A in Fig. 8). Each data point represents an average for the whole longitude band every 12 h. Figures 9a and 9b depict the time evolution of the zonal and meridional flows as a function of latitude. The NMC archiving of SOP II data began on 27 May, thus the gap in the NMC panel. The original GFDL analysis panel is whited out from 25° to 40°N due to extrapolation problems in the high terrain of the Tibetan plateau.

Fein and Kuettner (1980) noted on the summer MONEX (Monsoon Experiment) field phase that "the Indian monsoon of 1979 . . . was about two weeks late in arriving . . . onset at the southwest coast of India occurs normally on 1 June. . . ." From satellite

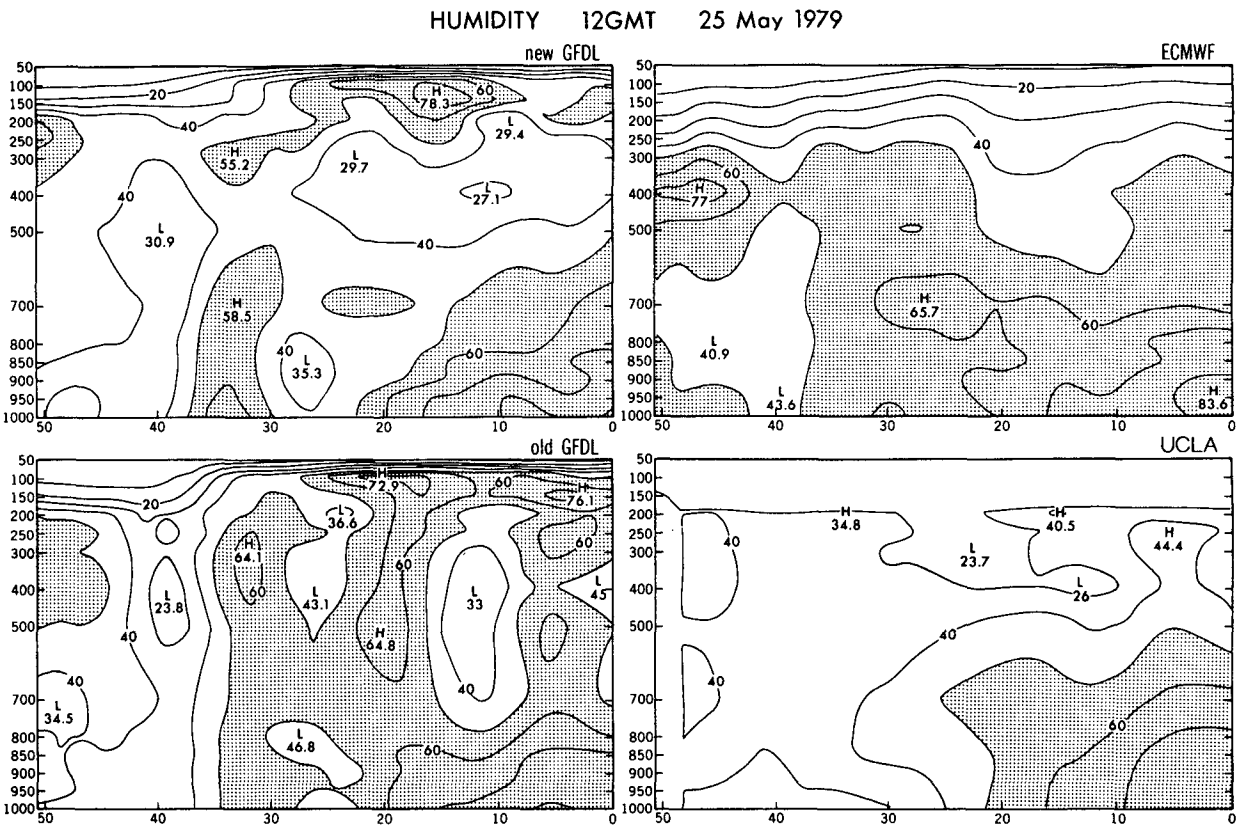

FIG. 7b. Same as Fig. 7a except for relative humidity (%). The contour interval is 10%. The regions in which the humidity is higher than 50% are stippled.

photos and other observations, Krishnamurti et al. (1981) determined that the monsoon onset vortex formed on 0000 UTC 14 June 1979 near 10°N. Krishnamurti (1985) states that "the onset vortex usually forms in the cyclonic shear side of the low-level jet in the lower troposphere over the eastern Arabian Sea, and that frequently, it moves meridionally towards the northern Arabian Sea." In Fig. 9a the mean zonal wind begins to increase from 29 May and reaches 5 m s^{-1} around 5 June in each panel; it attains 10 m s^{-1} near 12 June for almost all cases. All the analyses reach their maximum westerly wind near 17 June, except NMC, which reaches a higher maximum on 20 June. Each analysis has a corresponding easterly wind maxima at 17°N around 17 June yielding the maximum horizontal shear.

The time–latitude sections of zonally averaged meridional wind component at 850 hPa in Fig. 9b show the cross-equatorial flow increases around 12–13 June with maximum meridional wind near 18–19 June, just a day after the maximum zonal wind occurs.

Sikdar and Martin (1981) performed a similar analysis at 63° and 53°E utilizing analyzed low-level satellite cloud wind fields, and showed that a series of wind maxima of greater than 20 m s^{-1} occurred approximately 3–4 days apart (15, 18, 22, 25 June) at 13°N.

3. The accuracy of basic variables

Comparison of analyses with observations was performed by computing root-mean-square (rms) and mean differences between radiosonde observations and

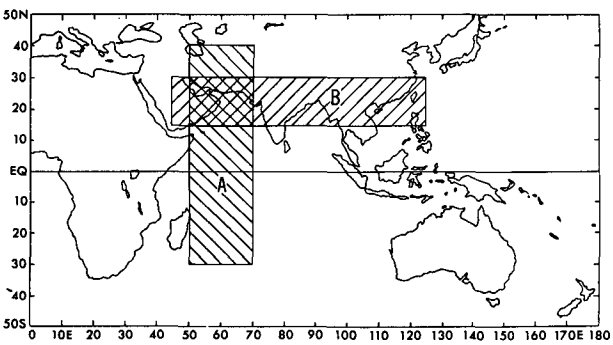

FIG. 8. The regions for studies of the onset of the Indian monsoon, box A (used for Fig. 9), and the vorticity and divergence, box B (used for Fig. 13).

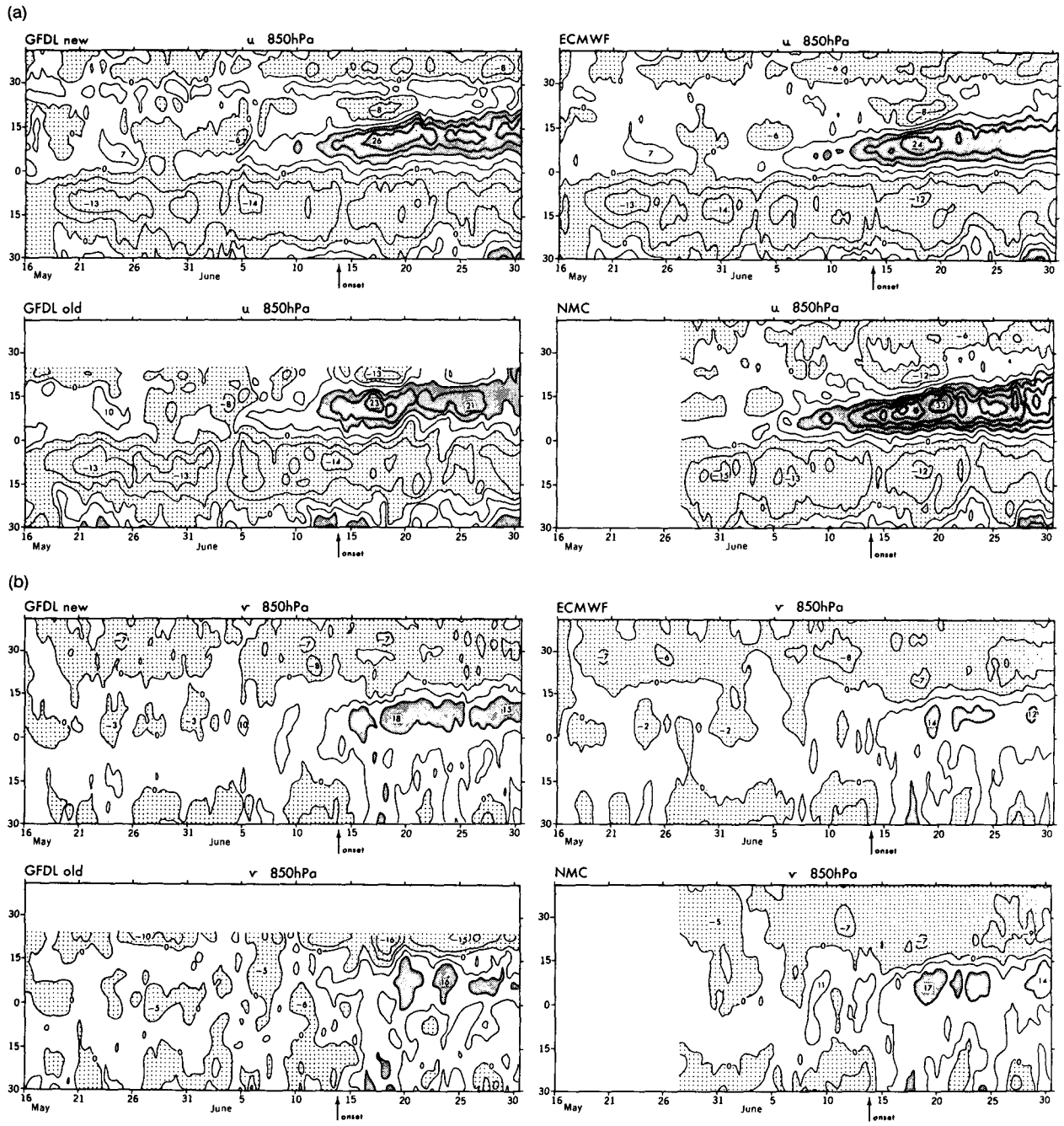

FIG. 9. (a) Time–latitude diagrams of zonal wind (m s^{-1}) at the level of 850 hPa. Areas of easterly winds are stippled, and areas of greater than 10 m s^{-1} are shaded. (b) The same as (a) except for meridional wind. Areas of northerly winds are stippled, and areas of greater than 10 m s^{-1} are shaded.

analyses at radiosonde stations. Four analyses are taken in this comparison: new GFDL, ECMWF, old GFDL, and NMC.

Figures 10a–c contain histograms of rms differences at standard pressure levels, 30–1000 hPa at 10-day intervals during SOP I over the Northern Hemisphere. Some general observations, looking at the rms temperature differences (Fig. 10a), show that in all but a few of the instances below 100 hPa the GFDL reanalysis has the smallest differences, and in all but five cases the GFDL reanalysis rms temperature differences are lower than the original GFDL, especially at the top level (30 hPa), where temperature and winds were not inserted in the original GFDL analyses. Something to be considered is the fact that the ECMWF and NMC analysis systems do not analyze for temperature but

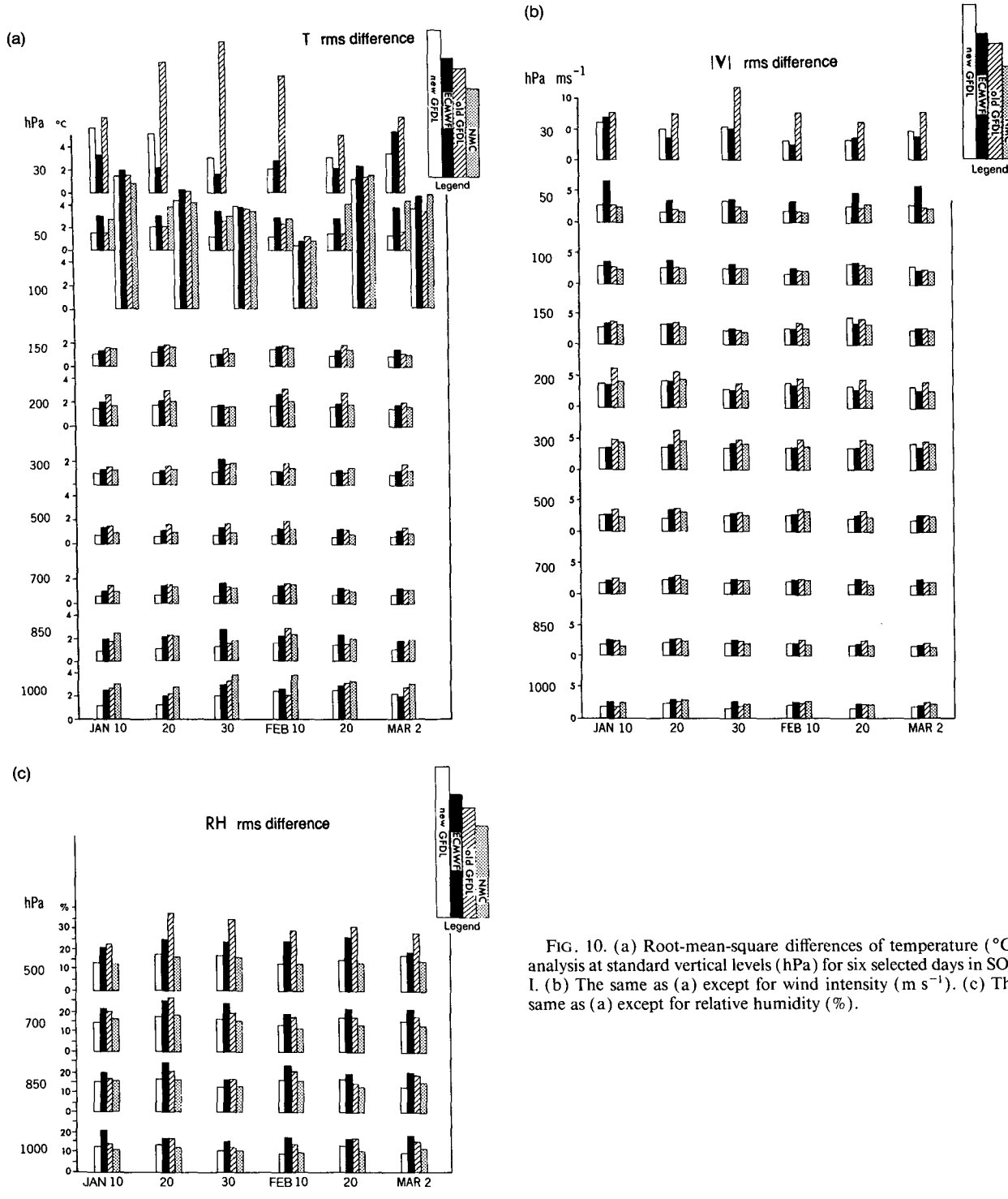

FIG. 10. (a) Root-mean-square differences of temperature (°C) analysis at standard vertical levels (hPa) for six selected days in SOP I. (b) The same as (a) except for wind intensity (m s^{-1}). (c) The same as (a) except for relative humidity (%).

for thickness. The magnitude of the rms temperature differences is largest at 100 hPa, just above the tropopause level.

Root-mean-square wind differences (Fig. 10b) are large in all analyses at the 200–300-hPa level, associated with the tropospheric jet. ECMWF rms wind differences are all larger than the other schemes at 50 hPa. In general, the original GFDL rms wind differences are larger than the GFDL reanalysis differences at all levels and times. Excluding the original GFDL, the other three analyses are all fairly similar in rms wind difference.

TABLE 2. The rms and mean analysis differences of geopotential height Z, temperature T, wind intensity ($|V|$), and relative humidity (RH). The tables are divided into SOP I and SOP II, for the Northern Hemisphere 75°–25°N and the tropics 25°N–25°S.

SOP I Northern Hemisphere

rms difference

	1000 hPa	850 hPa	500 hPa	300 hPa	50 hPa	30 hPa
			Z (m)			
Old GFDL	20.3	16.8	28.6	40.1	61.7	*82.5*
New GFDL	24.8	22.4	31.9	36.7	69.3	84.2
ECMWF	13.4	9.9	15.5	27.4	66.8	85.6
NMC	*12.9*	*9.0*	*13.6*	*23.2*	*59.4*	
			T (°C)			
Old GFDL	2.7	2.0	1.6	*1.6*	*1.9*	8.2
New GFDL	*2.5*	*1.6*	*1.2*	1.7	2.1	4.3
ECMWF	3.3	2.2	1.4	*1.6*	3.5	*2.8*
NMC	4.3	2.3	1.3	1.7	3.5	
			$\|V\|$ (m s^{-1})			
Old GFDL	2.8	2.9	3.7	5.3	*2.9*	7.9
New GFDL	*2.6*	*2.7*	3.5	5.3	3.3	5.5
ECMWF	3.1	2.9	*3.2*	*4.2*	4.9	*4.7*
NMC	3.0	*2.7*	3.5	4.7	*2.9*	
			RH (%)			
Old GFDL	14.8	17.1	32.8			
New GFDL	15.6	16.8	15.6			
ECMWF	17.9	19.1	24.5			
NMC	*10.4*	*14.0*	*13.9*			

Mean difference

	1000 hPa	850 hPa	500 hPa	300 hPa	50 hPa	30 hPa
			Z (m)			
Old GFDL	−4.6	−4.2	−9.5	−11.7	−6.4	−25.2
New GFDL	−8.6	−8.4	−15.3	−14.4	*−1.7*	*7.3*
ECMWF	2.0	2.1	−2.7	2.7	27.3	42.2
NMC	*0.0*	*0.7*	*−0.2*	*−0.3*	7.8	
			T (°C)			
Old GFDL	0.5	*−0.02*	*0.1*	*−0.05*	*−0.04*	−4.8
New GFDL	*−0.02*	−0.11	*0.1*	0.17	0.06	*−1.1*
ECMWF	1.2	0.3	0.4	0.3	2.4	1.7
NMC	1.7	0.2	0.12	0.4	0.27	
			$\|V\|$ (m s^{-1})			
Old GFDL	−0.3	−0.6	−0.6	−0.9	−0.2	1.4
New GFDL	*0.11*	−0.22	−0.3	−0.6	*0.03*	*0.4*
ECMWF	0.9	*−0.13*	*−0.12*	*−0.5*	1.9	0.7
NMC	0.7	−0.3	−0.3	*−0.5*	−0.2	
			RH (%)			
Old GFDL	*−0.7*	−3.1	−6.2			
New GFDL	6.1	−2.4	−2.3			
ECMWF	11.0	8.1	16.7			
NMC	*0.7*	*1.0*	*−0.1*			

SOP II Northern Hemisphere

rms difference

	1000 hPa	850 hPa	500 hPa	300 hPa	50 hPa	30 hPa
			Z (m)			
Old GFDL	17.2	15.8	25.7	34.5	58.6	*69.1*
New GFDL	19.0	18.6	26.4	33.6	64.2	79.7
ECMWF	*10.6*	*9.2*	*15.5*	*27.5*	*58.4*	74.8
			T (°C)			
Old GFDL	2.6	1.6	1.3	*1.5*	*1.6*	6.5
New GFDL	*2.2*	*1.4*	*1.0*	*1.5*	*1.6*	4.3
ECMWF	2.9	2.0	1.4	1.6	3.3	*2.9*
			$\|V\|$ (m s^{-1})			
Old GFDL	2.5	2.6	3.0	4.2	2.0	6.5
New GFDL	*2.3*	*2.4*	3.0	4.9	*1.9*	3.3
ECMWF	2.7	2.7	*2.9*	*4.0*	2.9	*2.8*
			RH (%)			
Old GFDL	*12.5*	11.7	28.7			
New GFDL	13.4	*11.5*	*16.4*			
ECMWF	16.9	17.7	22.3			

Mean difference

	1000 hPa	850 hPa	500 hPa	300 hPa	50 hPa	30 hPa
			Z (m)			
Old GFDL	−2.3	−2.6	−7.8	−10.0	*0.2*	*−11.8*
New GFDL	−5.4	−5.4	−11.3	−13.3	2.0	27.4
ECMWF	*−0.5*	*−1.3*	*−1.8*	*−2.7*	5.8	21.5
			T (°C)			
Old GFDL	0.6	*−0.04*	0.04	*0.11*	−0.23	−5.1
New GFDL	*0.1*	−0.12	*0.00*	0.14	*−0.16*	*−0.5*
ECMWF	−0.4	0.3	0.5	0.13	2.8	−2.3
			$\|V\|$ (m s^{-1})			
Old GFDL	−0.3	−0.7	−0.4	−0.7	−0.03	0.7
New GFDL	*0.08*	*−0.4*	*−0.3*	−0.9	*0.00*	*−0.14*
ECMWF	0.3	*−0.4*	*−0.3*	*−0.4*	−0.2	−0.9
			RH (%)			
Old GFDL	−2.8	−1.2	1.1			
New GFDL	*1.7*	*−0.2*	−2.8			
ECMWF	10.0	4.8	12.9			

TABLE 2. (*Continued*)

	SOP I Tropics						SOP II Tropics						
	rms difference						rms difference						
	1000 hPa	850 hPa	500 hPa	300 hPa	50 hPa	30 hPa		1000 hPa	850 hPa	500 hPa	300 hPa	50 hPa	30 hPa
			Z (m)							*Z* (m)			
Old GFDL	18.5	16.2	25.2	34.8	79.1	*85.5*	Old GFDL	15.5	15.4	23.3	*34.3*	*75.4*	*86.7*
New GFDL	23.0	21.2	30.0	40.4	87.7	92.4	New GFDL	19.0	19.9	24.5	34.7	80.3	92.1
ECMWF	15.8	11.8	23.1	36.0	90.8	96.8	ECMWF	*11.7*	*11.8*	*20.2*	34.8	89.2	107.6
NMC	*14.6*	*8.1*	*13.4*	*21.8*	*65.2*								
			T (°C)							*T* (°C)			
Old GFDL	2.0	1.4	1.2	*1.3*	*2.5*	6.7	Old GFDL	2.3	1.4	1.2	1.4	*2.5*	6.6
New GFDL	*1.5*	*1.0*	*0.9*	1.4	2.6	4.9	New GFDL	*1.4*	*1.1*	*0.9*	*1.2*	*2.5*	4.7
ECMWF	2.2	1.7	1.7	1.7	3.9	*3.6*	ECMWF	2.3	1.6	1.6	1.6	3.9	*3.9*
NMC	2.8	2.3	1.3	1.5	5.6								
			|V| (m s^{-1})							|V| (m s^{-1})			
Old GFDL	2.3	2.4	2.7	3.9	3.3	6.1	Old GFDL	2.1	2.3	2.4	3.3	2.9	8.9
New GFDL	2.2	2.2	2.6	4.1	3.8	*5.7*	New GFDL	*2.0*	*2.2*	*2.2*	3.6	*2.7*	*5.0*
ECMWF	2.2	2.8	2.7	3.7	7.2	12.3	ECMWF	2.4	2.7	2.6	*3.1*	7.8	9.1
NMC	*2.1*	*1.9*	*2.1*	*3.2*	*2.8*								
			RH (%)							RH (%)			
Old GFDL	10.5	12.5	29.0				Old GFDL	10.6	10.7	30.3			
New GFDL	9.7	13.8	*11.6*				New GFDL	*8.4*	*10.5*	*13.9*			
ECMWF	*10.0*	*16.4*	16.9				ECMWF	9.8	15.6	18.3			
NMC	*8.0*	*11.7*	12.7										
	Mean difference						Mean difference						
	1000 hPa	850 hPa	500 hPa	300 hPa	50 hPa	30 hPa		1000 hPa	850 hPa	500 hPa	300 hPa	50 hPa	30 hPa
			Z (m)							*Z* (m)			
Old GFDL	−2.8	*−2.5*	−2.7	−4.9	19.1	*−4.4*	Old GFDL	−2.1	*0.4*	3.4	*2.3*	13.5	−12.2
New GFDL	−6.2	*−7.0*	−13.1	−18.5	13.8	5.1	New GFDL	−4.2	−3.9	−3.9	−7.8	*10.3*	*4.5*
ECMWF	−1.4	*−3.3*	*−2.5*	*0.4*	−10.3	−30.5	ECMWF	*−0.5*	−1.4	*0.7*	4.9	−10.9	−28.1
NMC	*0.7*	*−0.8*	*−2.5*	−3.8	*−1.4*								
			T (°C)							*T* (°C)			
Old GFDL	0.48	0.18	0.24	*0.02*	−0.93	−3.09	Old GFDL	0.7	0.3	0.22	0.14	−0.7	−3.7
New GFDL	*−0.23*	*−0.02*	*−0.07*	−0.07	*−0.62*	*−1.44*	New GFDL	*−0.07*	*0.08*	*0.09*	*0.02*	*−0.4*	*−1.0*
ECMWF	0.71	0.22	0.18	0.15	2.33	1.89	ECMWF	0.7	0.5	0.5	*0.02*	1.9	2.0
NMC	1.64	1.35	0.27	−0.07	−3.35								
			|V| (m s^{-1})							|V| (m s^{-1})			
Old GFDL	*0.02*	−0.49	*−0.26*	−0.47	*−0.29*	−0.62	Old GFDL	*0.14*	−0.4	*−0.2*	−0.5	−0.1	−4.4
New GFDL	0.40	*−0.12*	−0.29	*0.00*	−0.35	*0.43*	New GFDL	0.4	*−0.15*	−0.3	*−0.3*	0.27	*−0.9*
ECMWF	0.89	−0.58	−0.31	−0.51	2.16	4.34	ECMWF	0.7	−0.7	−0.6	−0.7	3.1	2.3
NMC	0.14	−0.59	−0.44	−0.35	−10.6								
			RH (%)							RH (%)			
Old GFDL	−1.4	−1.7	7.8				Old GFDL	*−1.7*	−1.7	*0.9*			
New GFDL	4.0	−3.6	−2.9				New GFDL	2.8	*−1.6*	−1.7			
ECMWF	*1.1*	5.2	5.8				ECMWF	2.0	4.1	6.9			
NMC	−1.6	*1.0*	*1.1*										

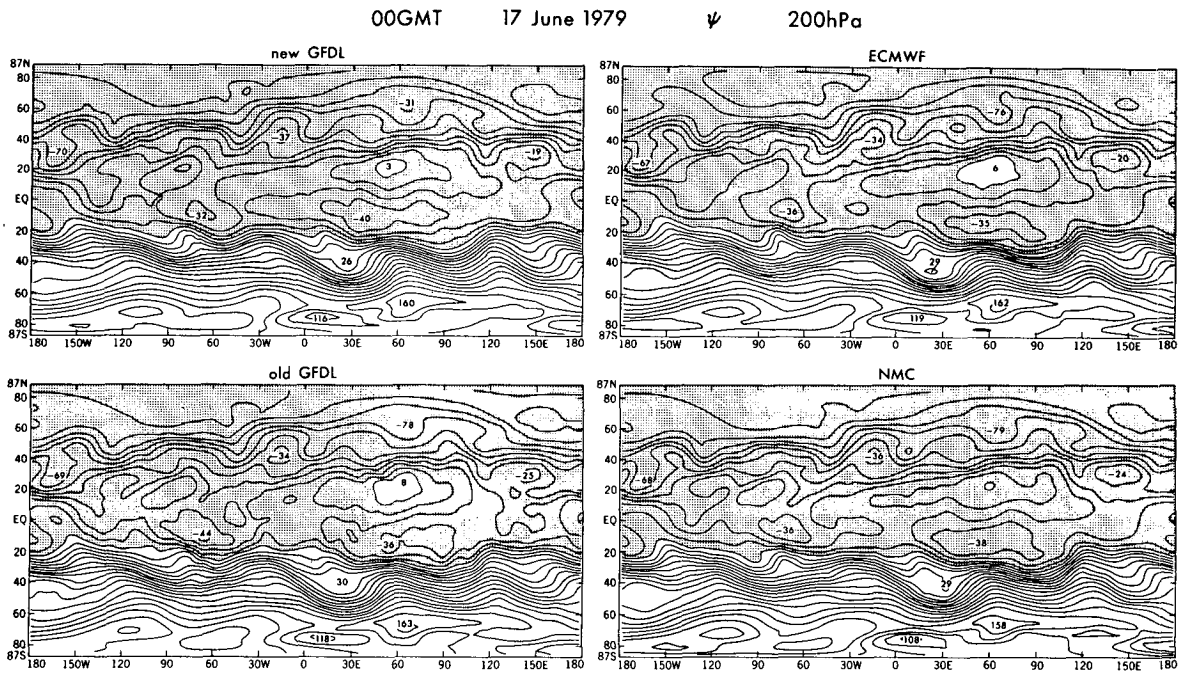

FIG. 11. Longitude–latitude maps of 200-hPa streamfunction Ψ. Units are $10^5\ s^{-1}$. Contour interval is $10 \times 10^5\ s^{-1}$. The negative regions are shaded.

With the exception of 20 February at 850 hPa, the GFDL reanalysis is lower in rms relative humidity difference (Fig. 10c) than the original GFDL, especially at 500 hPa. The original GFDL and ECMWF are both consistently larger than the GFDL and NMC reanalyses.

Table 2 displays the average of 12 times (at 5-day intervals), during SOP I and II, of rms and mean differences for 518 Northern Hemisphere stations (25°–75°N), and 145 tropical stations (25°S–25°N). The smallest differences in each vertical column among the four analyses are italicized. A similar comparison over 110 North American stations gave results comparable to the Northern Hemisphere statistics.

The ECMWF and NMC rms geopotential height differences (Z in Table 2) are lowest across the board. Also, NMC relative humidity differences (RH in Table 2) are lowest across the board, except for 500 hPa during SOP I in the tropical belt. GFDL reanalysis rms and mean temperature differences are the lowest at 500 hPa and below during both SOPs.

In the Northern Hemisphere, the ECMWF mean relative humidity differences are quite a bit larger than the others. In the tropics, though, this is not always the case. The GFDL reanalysis tends to have a positive bias of relative humidity at 1000 hPa and a negative bias at 850 and 500 hPa. Moisture appears to be confined to lower levels.

In the tropics, the two GFDL analyses seem to have the lowest mean wind differences at all levels for both SOPs, while NMC has the lowest rms differences at all levels for SOP I. Undén (1989) noted that an important limitation of the ECMWF wind analyses, particularly in the tropics, was the use of a nondivergent constraint on the wind-analysis increments. When a part of the divergence was included, tropical wind observations were analyzed more faithfully.

Thus, the difference study based on the verification against radiosonde observations has revealed that in general, temperature and wind differences (both rms and mean) have improved considerably from the original to the reanalyzed GFDL analyses, and that with regard to the geopotential height, both rms and mean differences were larger in the reanalyzed GFDL than in the original for an undiscovered reason, while ECMWF and NMC predominantly had the lowest differences.

4. Derived variables

a. Streamfunctions and velocity potentials

The streamfunctions Ψ at 200 hPa for 0000 UTC 17 June are compared among the four analysis sets in Fig. 11. In the original analyses (Lau 1984a) it was shown that they are reasonably close to each other. On the other hand, the velocity potential χ is one of the most difficult variables to analyze accurately (Ploshay et al. 1984). The fields of χ at 200 and 850 hPa for the same time are compared in Figs. 12a,b. The divergent wind direction is perpendicular to the χ contours from lower toward higher values. Negative regions of χ at 200 hPa are associated with rising motion, while neg-

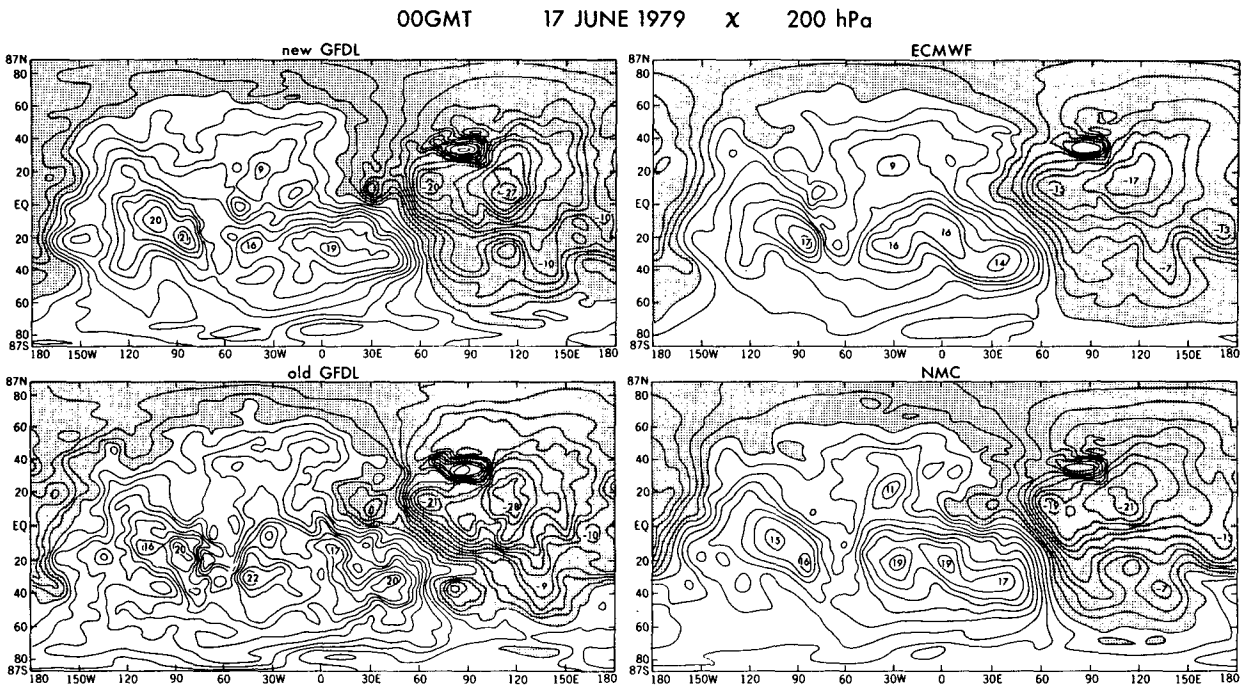

FIG. 12a. 200-hPa velocity potential χ. Units are 10^6 s^{-1}. Contour interval is 2×10^6 s^{-1}. The negative regions are shaded.

ative regions of χ at 850 hPa are associated with sinking motion.

It is encouraging to see that the various analyses have become more similar to each other in the FGGE reanalyses as compared to the original analyses. So far as the GFDL analyses are concerned, the new analysis is substantially smoother than the old GFDL, and it resembles the ECMWF or the NMC more than the old

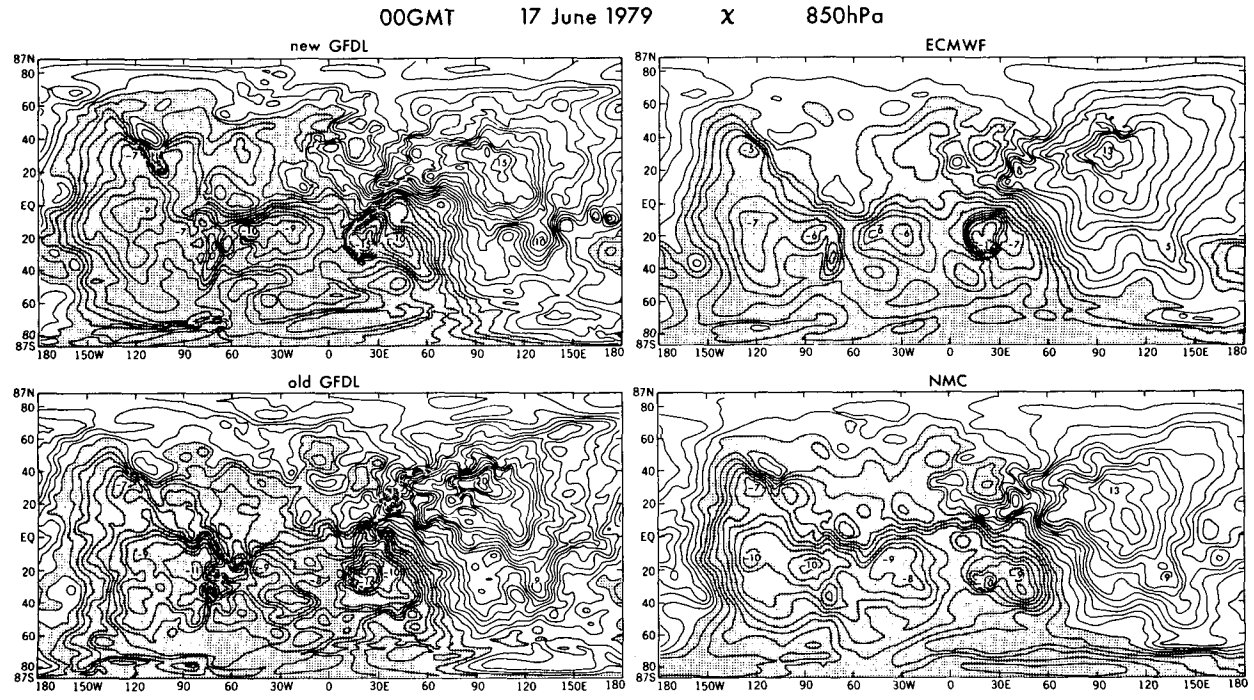

FIG. 12b. The same as in Fig. 12a except for 850 hPa.

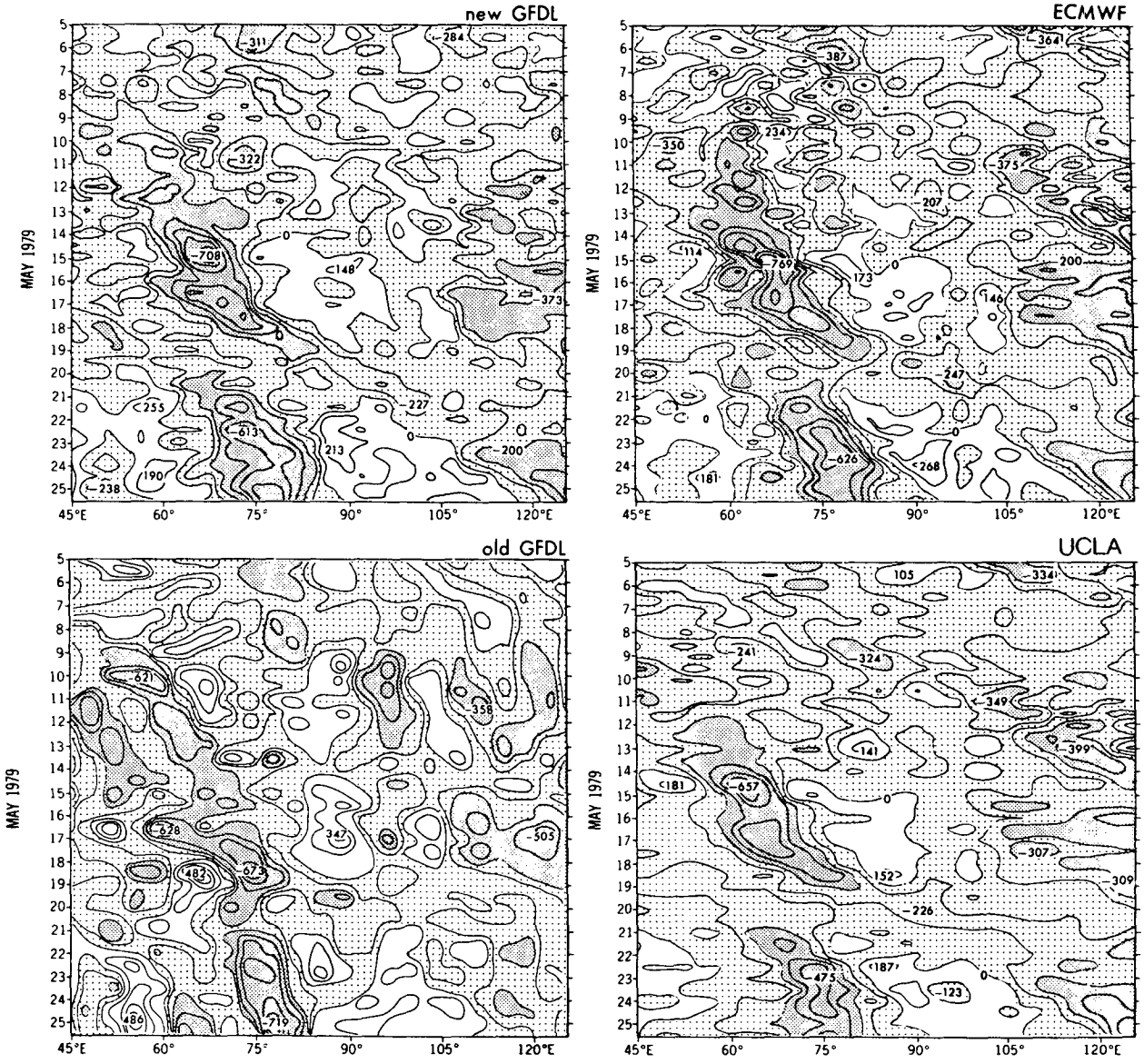

FIG. 13a. Longitude–time diagram of meridionally averaged vorticity. The contour intervals are 10^{-2} s^{-1}. Dark stippling indicates the areas of vorticity less than -2×10^{-2} s^{-1}, and light stippling indicates those larger than 0 s^{-1}.

GFDL. Inspection of maxima and minima in Figs. 12a,b reveals that the intensities are, in decreasing order: the old GFDL, the new GFDL, the new NMC, the new ECMWF, and the old ECMWF (the last one is not shown here). The degree of smoothness of the χ fields is in just the opposite order to the intensity. However, it is not known which is more accurate.

b. Hovmöller diagrams of vorticity and divergence

In section 2, the Yanai analysis is compared with the GFDL and ECMWF reanalyses and the original GFDL analysis. Here in Fig. 13 a quantitative comparison is made, taking statistics latitudinally averaged between 15° and 38°N, shown in box B of Fig. 8. The variables selected are the vorticity and divergence. Figures 13a and 13b display the Hovmöller diagrams (longitude–time charts) of vorticity and divergence at 200 hPa. The three reanalyses resemble each other reasonably well for the vorticity, and to a lesser extent, for the divergence with the original GFDL bearing the least resemblance.

In order to have a quantitative assessment of the resemblance, the linear correlation coefficients of pairs among the four fields in Figs. 13a,b, and the rms differences of pairs are calculated (Table 3). For vorticity

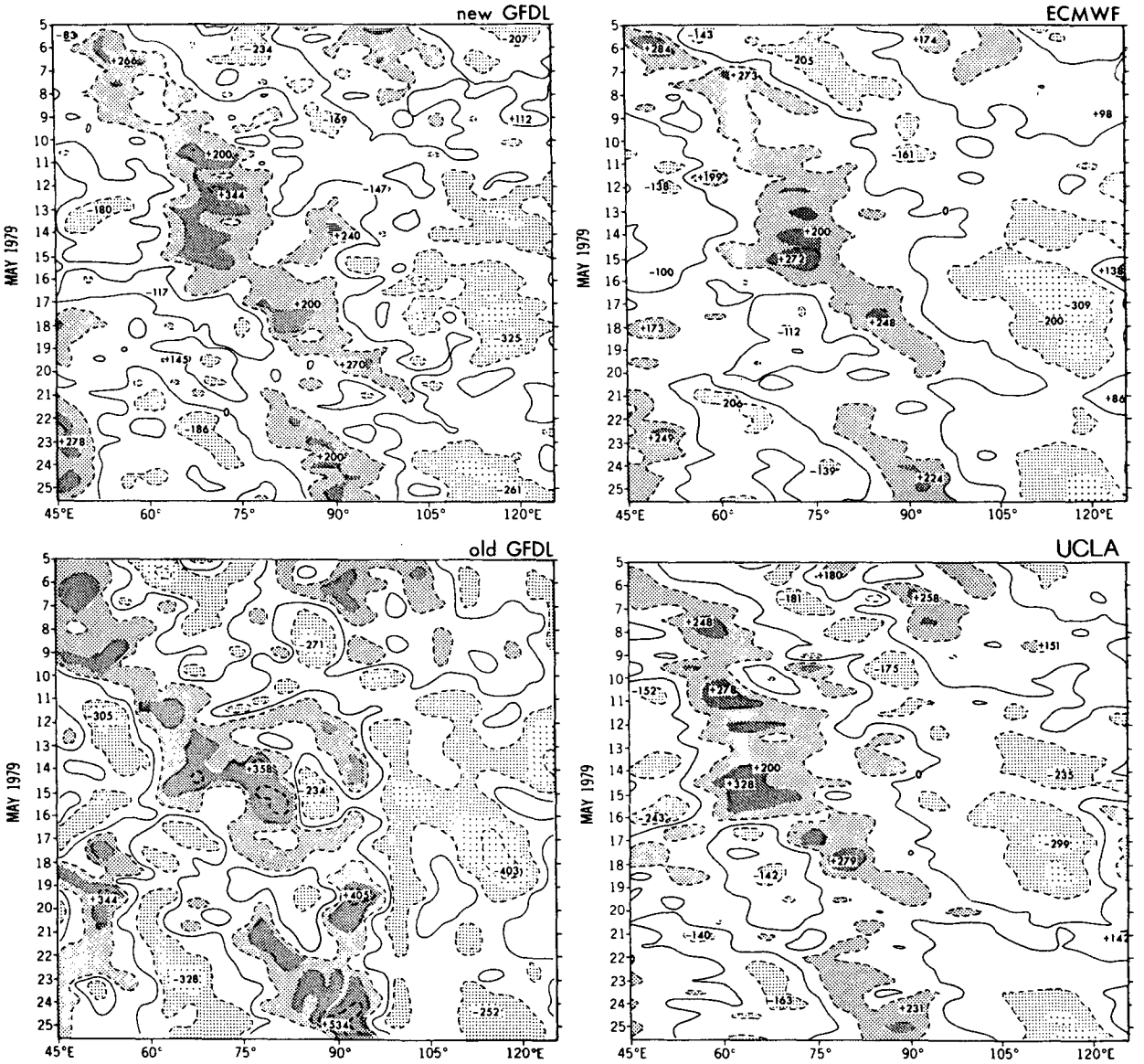

FIG. 13b. The same as in Fig. 13a except for divergence. Dark stippling is for greater than 2×10^{-2} s^{-1}, medium for between 2×10^{-2} s^{-1} and 10^{-2} s^{-1}, light for between -10^{-2} s^{-1} and -2×10^{-2} s^{-1}, and the lightest for less than -2×10^{-2} s^{-1}.

the three reanalyses are closely correlated, though the highest correlation is between the GFDL and ECMWF reanalyses with the original GFDL being least correlated to any of the others. The rms differences are lowest between the ECMWF and Yanai. In terms of divergence, the highest correlation and lowest rms differences are between the ECMWF and reanalyzed GFDL.

c. *Madden–Julian oscillations*

One of the outstanding discoveries in the FGGE activities was the finding of Madden–Julian oscillations (30–60 day) in the data assimilation (Lorenc 1984). It is indeed intriguing to see such a unique capability in data assimilation, despite the fact that models are not necessarily capable of producing these oscillations in their own simulations.

These oscillations are known to be Kelvin waves selectively modified by condensational heating, thus propagating eastward in the tropical region close to the equator with 30–60-day periods (Lau and Peng 1987; Tokioka et al. 1988). It has become a yardstick for a data-assimilation scheme on whether it is capable of representing these tropical disturbances adequately, because spurious gravity oscillations may be generated in data assimilation, and its separation from the real gravity waves may be difficult.

Figure 14 is a Hovmöller diagram of velocity poten-

TABLE 3. Correlation coefficients (upper right) and rms difference (s^{-1}, lower left) between pairs for vorticity and divergence.

Vorticity					
	New GFDL	ECMWF	Yanai	Old GFDL	
New GFDL		.71	.65	.47	Correlation
ECMWF	1.01×10^{-5}		.70	.49	
Yanai	1.04×10^{-5}	0.99×10^{-5}		.43	
Old GFDL	1.49×10^{-5}	1.47×10^{-5}	1.47×10^{-5}		
	rms				
Divergence					
	New GFDL	ECMWF	Yanai	Old GFDL	
New GFDL		.73	.58	.53	Correlation
ECMWF	0.75×10^{-5}		.66	.55	
Yanai	0.95×10^{-5}	0.81×10^{-5}		.53	
Old GFDL	1.20×10^{-5}	1.14×10^{-5}	1.18×10^{-5}		
	rms				

tial anomalies χ' from the time mean $\bar{\chi}$: at 300 hPa in the zonal belt between 10°N and 10°S. The anomalies are the components of χ remaining after subtraction of geographically persistent features $\bar{\chi}$:

$$\chi'(\lambda, t) = \chi(\lambda, t) - \bar{\chi}(\lambda)$$

where $\bar{\chi}$ is the time mean from 5 May to 30 June 1979 for the respective longitude λ. The linear temporal trend has not been removed.

The data assimilations for the new GFDL, the ECMWF, and the old GFDL are displayed. The observed OLR (outgoing longwave radiation) is also treated in a similar way as χ, and its Hovmöller diagram is shown in Fig. 14. An equal-weighted three-point time smoothing has been applied to the OLR data.

Even over this short time period of anomaly computation, an apparent 30–60-day oscillation appears in all of the data assimilations, while it is somewhat less obvious in the observed OLR anomaly. It is interesting to see that intensification of the χ and OLR anomalies can be seen near the time of the formation of the monsoon onset vortex in the Arabian Sea (0000 UTC 14 June 1979 at 60°E).

5. Remarks

a. Time evolutions of three variables

In Figs. 15a,b, the time evolutions of three variables are displayed for the reanalysis time period of SOP I. One is the squared vertical pressure velocities ω^2 averaged over the zonal belt of 24°N–24°S and integrated vertically, and the others are the 12-h rates of precipitation and evaporation, averaged over a global domain. Two curves for ω^2 are plotted in Fig. 15a; one is ω^2 for the data assimilation and the other is for the 6-h forecasts, that is, the first guess. There are also two curves in Fig. 15b; one is the rate of precipitation, and the other is the rate of evaporation, both averaged over the globe in the data assimilation.

The degree of separation between the solid and dashed lines of ω^2 (the assimilations and forecasts) decreases, after 28 January in SOP I, at which point the toss-out criteria for the quality control of observations were tightened. Retrospectively, this tightening was overdone and more data were rejected than necessary (mostly satobs and aireps, not radiosonde data). The fact that the solid lines are generally higher than the dashed lines may reveal that an excessive number of fast modes are generated by the injection of observational data. An iteration method such as the forward–backward process may reduce this discrepancy (this is the genuine four-dimensional analysis defined by McPherson 1975). The closeness between the ω^2 lines may indicate that the spinup in our data-assimilation system is not serious, but is in fact satisfactorily handled.

Concerning the relationship between the solid and the dashed lines in Fig. 15b, the rates of precipitation are almost always less than those of evaporation. This suggests that there is a moisture sink in this data-assimilation system. Since the system is not closed, there is the possibility that the injected observational moisture data are lower than the values in the GCM. Or, for example, the model's criterion for condensation might be the cause for the source or sink; the saturation relative humidity is specified as 100%.

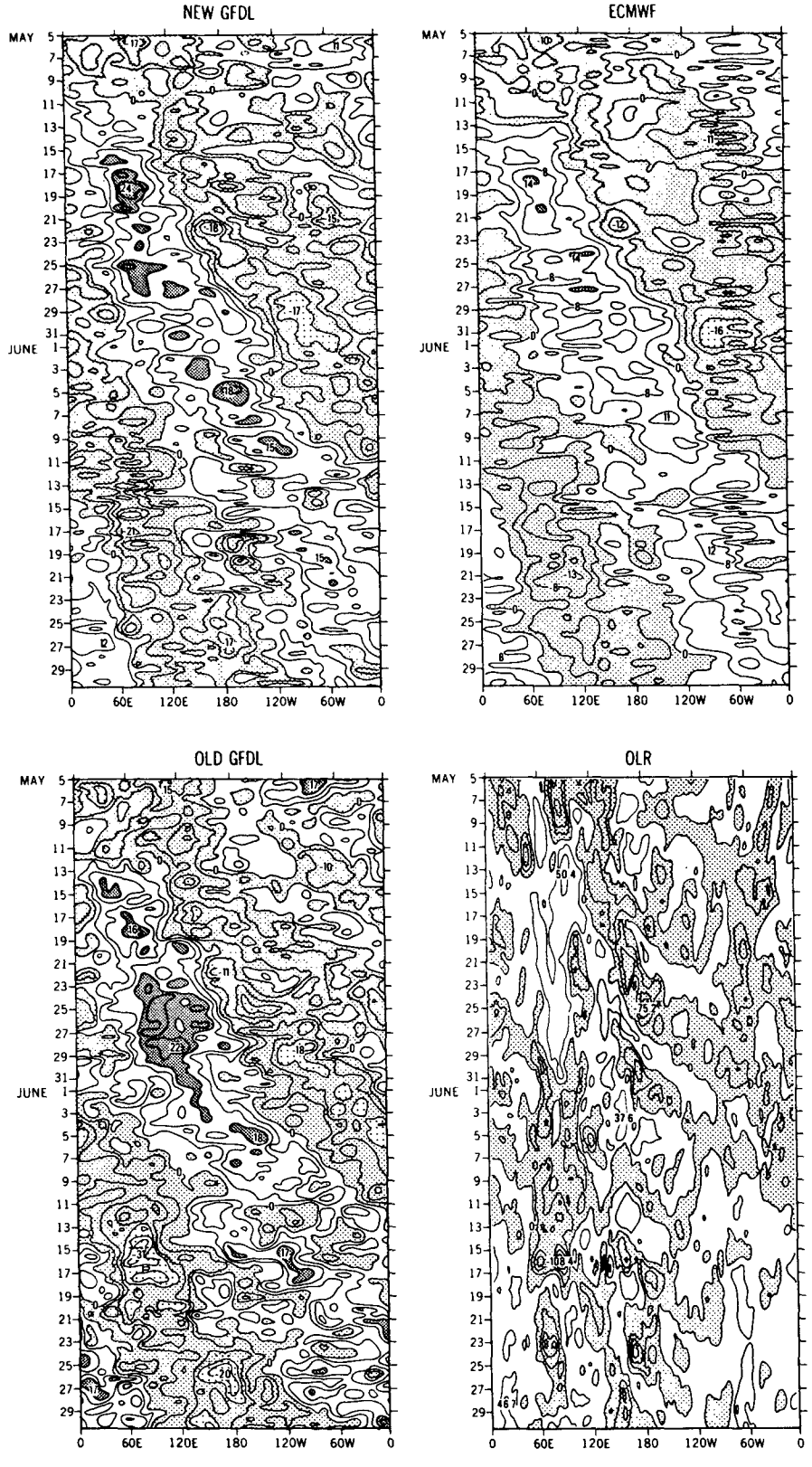

FIG. 14. Time–longitude diagrams of meridionally averaged (10°N–10°S) velocity potential anomalies at 300 hPa, for three analyses (the contour interval is 4×10^6 m^2 s^{-1}), compared with the observed OLR diagram (the contour interval is 40 W m^{-2}).

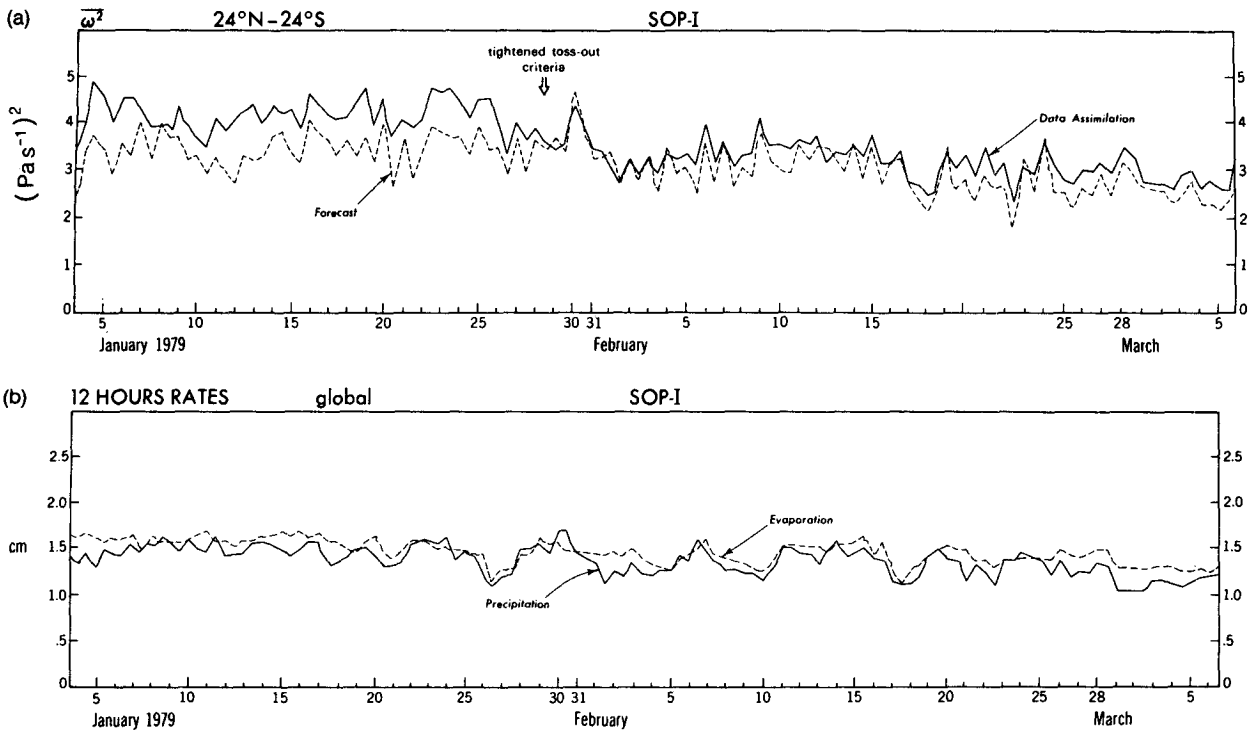

FIG. 15. (a) Time series of ω^2 (Pa s^{-1})^2 for the tropic during SOP I. The solid lines are for the data assimilation and the dashed lines are for the first guess, i.e., 6-h forecast. (b) Time series of 12-h rates of global precipitation [cm (12 h)$^{-1}$, solid lines] and evaporation (dashed lines) in SOP I.

b. Lenient toss-out criterion of wind data

It was alluded to earlier that occasionally appreciable discrepancies appear between the new GFDL and the new ECMWF analyses. After examination, it has been revealed that some wind-observation data have not been utilized, but discarded. Figures 16 and 17 show two examples, which belong to the cases just described.

Figure 16 is the case mentioned in Hollingsworth et al. (1985) and discussed in section 2 and Figs. 5 and 6. The panels on the left (both top and bottom) display how many wind-data observations were used in the new GFDL analysis. The wind data that were rejected even in the new GFDL analysis are enclosed by single and double circles. The data assimilation based on this selection of wind data was already shown in Figs. 5 and 6. By taking a more lenient criterion for quality control, an additional experiment was conducted. The wind data enclosed by single circles are now utilized in this experimental data assimilation. The resultant wind fields are displayed in the panels on the right-hand side. The assimilation in this experiment had started two days before the time in this figure, using the more lenient criterion. It is seen that the new analyses have come closer to the new ECMWF (Fig. 6).

The newly accepted data are exclusively satobs and aireps. Accepting single-level, sparse wind observations, such as in this situation, requires either a better first guess or a more lenient acceptance of data, which would increase the risk of accepting some spurious data. The problem with the first guess in this case was that it was determined by a forecast from an analysis with equally sparse data 6 h earlier. In data-rich areas, such as over the continental United States, there is much less of a problem. As seen in the left panels of Fig. 16, there are still a large number of wind data that have not been utilized (double circles); they are also satobs and aireps, except one radiosonde data at 46°N, 150°E.

Figure 17 is the case of the comparison with the UCLA analysis, which was discussed in section 2 and in Figs. 8a,b. The results of experimental analysis using the more lenient criteria are shown in Fig. 17. As is seen, the maximum intensity of zonal wind has increased from 28.6 to 36.5 m s^{-1}, where that of the new ECMWF is 35.5 m s^{-1}. It should be noted, however, that the temperature and humidity analysis have not been noticeably affected by the inclusion of extra data.

The reason that the tighter criterion was chosen for wind in the new GFDL analysis is described later. During a case study on 0000 UTC 7 January 1979, it was discovered that a fictitious temperature and sea level pressure trough had developed near the British Isles. One sounding (station 3920 at 54.48°N, 6.10°E) from a radiosonde reported a 10°C temperature jump at the surface, in just the first few moments of flight. This 10°C error was not determined to be erroneous by the

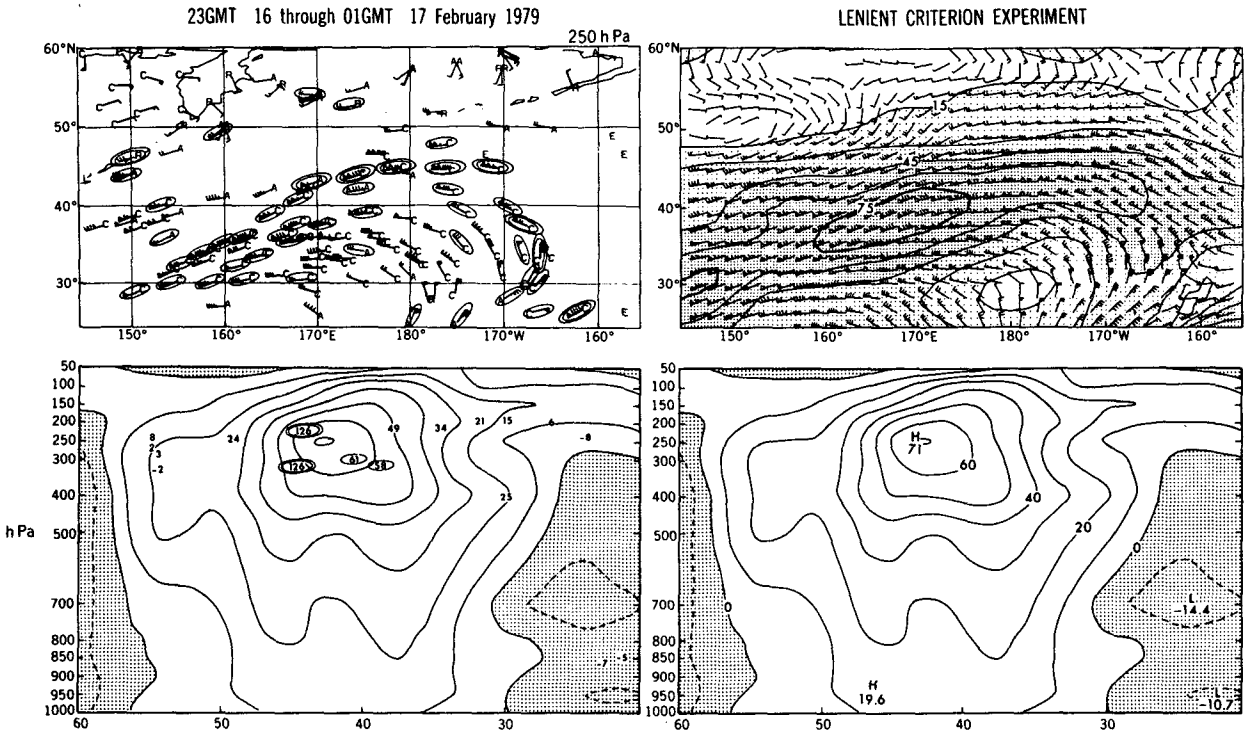

FIG. 16. An example to show the impact of discarded data on the analysis for 0000 UTC 17 February 1979. The upper left panel displays various wind observations in the horizontal domain at 250 hPa, and the lower left panel indicates wind observations along the date line in the latitude–height section. The wind arrows labeled A are aireps, C are satobs (cloud winds), and R are radiosonde data. The upper right is the wind analysis in the additional experiment using more lenient toss-out criterion, which is to be compared with the new GFDL analysis in Fig. 4. The lower right is the isotach analysis in the additional experiment, which is to be compared with the new GFDL analysis in Fig. 5. Aircraft *40614* observations cross the middle of the upper left panel from 165°E to 165°W.

analysis scheme, because the temperature cutoff was a 24°C departure from the first guess. Consequently, the cutoff selection criteria for all variables were dramatically reduced. Our reductions in temperature cutoffs were reasonable; however, the proportional reductions in wind cutoff criteria were too drastic and actually unnecessary.

Since the cutoffs were tightened beginning with the 0000 UTC 28 January 1979 analysis time, the GFDL 200-hPa January mean zonal winds (Fig. 3) have not been adversely affected. Subsequently, in February, jet-level winds in the region bounded by 20°–30°N, 100°–130°E were about 10% weaker than the ECMWF and NMC reanalyses. A similar weakening occurs in the jet-level winds in the Southern Hemisphere in the May and June reanalyses at almost every analysis time. The too-tight data-selection criteria created a feedback effect to the forecast first guess, causing even some radiosonde data over China to be rejected. Application of our current scheme with lenient selection criteria and a buddy check has eliminated this problem.

In summary, the impact of the more lenient criteria for wind-data quality control appears to primarily affect the analysis at the tropospheric jet level. Hence, the effect due to excessive discarding of satobs and aireps would not be extensive, although ω^2 was noticeably modified (Fig. 15a).

c. *Iterative continuous method*

As was mentioned associated with Figs. 1a,b, even in the revised data assimilation scheme (Stern and Ploshay 1992), the fast modes are still excessively generated by the injection of observational data. Perhaps a more serious drawback in the current continuous data-assimilation system is that a large amount of fictitious condensational heating is generated every 6 h by the insertion of massive amounts of new observation data, and as a result, the diabatic variables obtained in the assimilation cannot be utilized as reasonable archival components of the dataset (Salstein, personal communication).

This deficiency may be resolved by applying a second iteration of data injection, that is, the forward–backward scheme, as was discussed by Miyakoda et al. (1978), though in that paper's proposed scheme the "Euler backward" scheme is replaced by the "linear normal-mode balancing" for the incremental part of observation data (Daley and Puri 1980). Along the line of the forward–backward scheme, an interesting

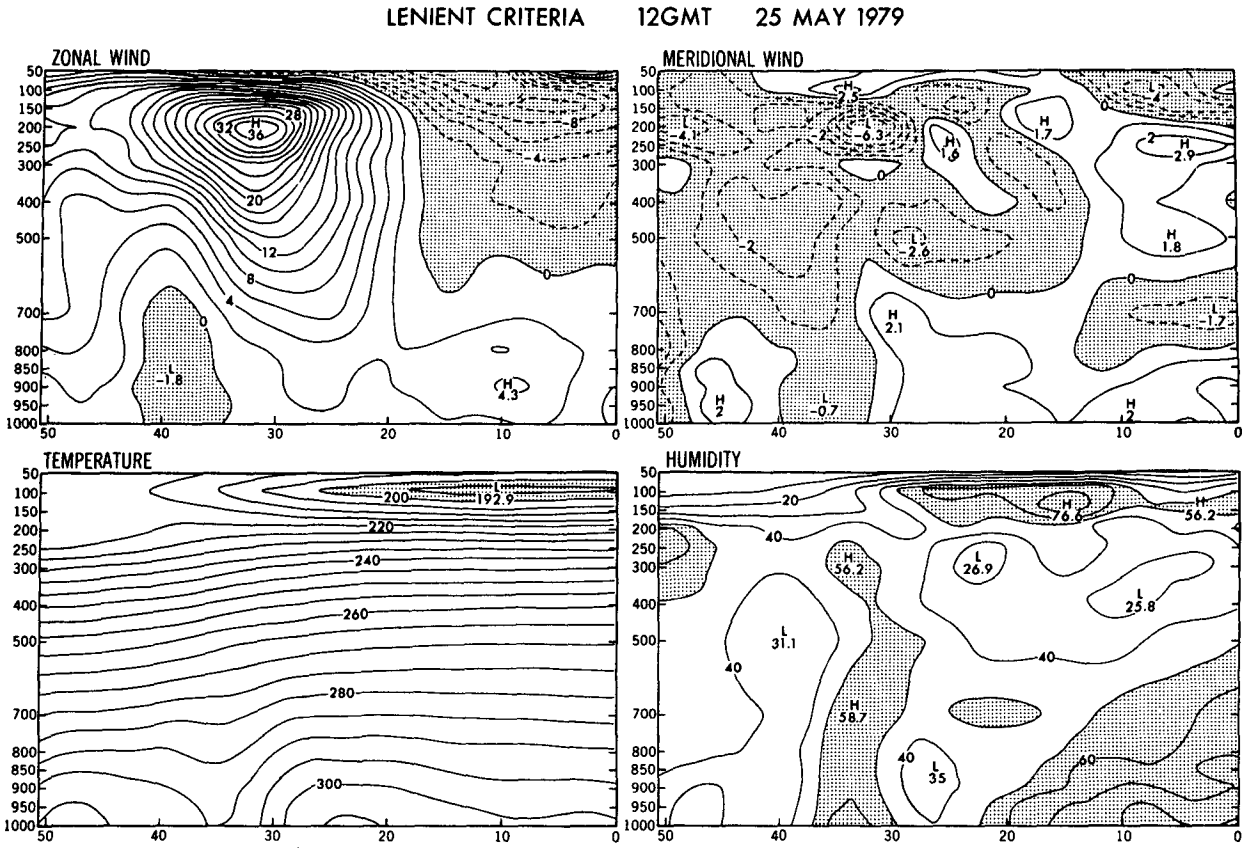

FIG. 17. Analysis of the additional experiment for 1200 UTC 25 May 1979, using more lenient criteria for data rejection. The upper left (zonal wind) is to be compared with the upper left in Fig. 7a. The lower right (humidity) is to be compared with the upper left in Fig. 7b. The upper right (meridional wind) and the lower left (temperature) are attached.

study has been carried out by Fox-Rabinovich and Gross (1990), though this is not the continuous-injection method.

6. Summary and conclusions

Using the revised data-assimilation system at GFDL, a reanalysis of the FGGE dataset has been performed for two special observation periods. The new analysis uses the continuous data-insertion technique similar to the original analysis. However, the first guess is the 6-h forecast in the new system, as opposed to the 12-h persistence in the old system, and the data-collection range is now 500 km, in contrast to 250 km. The spatial resolution of the GCM is increased from R30 to R42. The data initialization (dynamical balancing) is the linear normal-mode method, which is applied every time step only to the incremental part of the observation beyond the first guess for modes with periods less than 6 h, whereas in the original system nonlinear normal-mode initialization was applied every 6 h to the full fields after the optimum-interpolation (OI) analysis, though the components with periods longer than 6 h were not initialized.

The reanalysis reveals that the new GFDL data assimilation has come closer to the new ECMWF assimilation in terms of the features of various contour maps, the accuracy of representing observations, and the smoothness of analysis patterns. The new GFDL analysis resembles that of the new NMC as well. In particular, maps of all variables exhibit considerable reduction of noise, compared with the original GFDL analysis, implying that there is a greater consistency in the mass and wind fields in the new analysis. The divergence fields are more similar to each other among the revised analysis of GFDL, ECMWF, and NMC. The intensity of tropical vertical velocities is, in descending order, original GFDL, new GFDL, new NMC, new ECMWF, and original ECMWF. At this moment, it is not clear which one is most correct.

The analysis of the Southern Hemisphere has been improved, and three analyses, that is, new GFDL, new ECMWF, and new NMC, have come closer to each other (Ploshay et al. 1990). Another aspect is that the

original GFDL analyses exhibited occasionally weaker cyclone patterns; this type of error has been significantly alleviated. This was shown in Stern and Ploshay (1992) and Stern et al. (1985) via the analysis of the Presidents' Day snowstorm (February 1979), a fast-moving and rapidly deepening midlatitude cyclone in a data-sparse region, which was represented much better in the new GFDL analysis than in the original GFDL analysis. This has been accomplished largely due to the better first guess and the data assimilation with less strict dynamical balancing, which resulted in much greater acceptance of good observations.

The new GFDL analyses are compared with the objective analyses of UCLA over the Asian summer monsoon region. Comparison is also made with the new ECMWF analyses over this region. All analyses agree reasonably well in terms of the magnitude of vorticity and divergence in their daily variations.

However, it should be pointed out that three aspects are still deficient. One is the excessively tightened rejection criterion for wind; the second is the analysis of moisture; and the third is the derived diabatic variables. The first point is that the satobs and the aireps were excessively tossed out, and as a result, the wind maximum at the tropospheric jet level has been reduced appreciably. In view of the imperfect quality of general circulation models (GCMs), more lenient toss-out criteria are desirable. Second, the analysis of moisture is still considerably different for various centers' systems, as was pointed out for the original FGGE analysis by Chen and Lee (1984). It appears that this aspect can be rectified only through the improvement of cumulus parameterization together with the specification of clouds in GCMs, and also improvements to the boundary-layer parameterization. Third, in order to improve the archived diabatic variables, the variables in the first 2 h every 6 h should be filtered out properly, because the diabatic variables in this period are disturbed by injection of new data. The remedy may be to develop an iteration procedure in the data assimilation.

In summary, one of the important conclusions is that forward continuous data assimilation works well with an incremental linear normal-mode initialization applied each time step. The dynamical balancing applied here is less strict than the nonlinear normal-mode initialization. This implies that the continuous system should have fewer difficulties in the spinup problem, which has been one of the issues in the intermittent type of data assimilation.

Acknowledgments. The authors wish to thank Bill Bourke, Kamal Puri, and Prof. M. Yanai. Robert White, Bruce Wyman, George Vandenberghe, and Robert Smith helped to process the analyses. The completion of this project has taken a considerable amount of time. We appreciate the patience of the administrators, Dr. J. Smagorinsky and Dr. J. Mahlman. Assistance from outside of GFDL is acknowledged: for example, Prof. F. Baer, Dr. D. A. Salstein, Dr. D. Ballish, and Prof. E. Kung. We also thank Phil Tunison and his staff for drafting the figures and Wendy Marshall for typing the manuscript.

REFERENCES

Arpe, K., 1984: Fit of FGGE level III-b analyses by ECMWF and by GFDL to observational data during the period 27 February to 7 March 1979. *GARP Special Report* No. 44, WMO/ICSU, Report of the seminar on progress in tropical meteorology as a result of the global weather experiment at Tallahassee, FL, pp. I-36–45.

Bengtsson, L., M. Kanamitsu, P. Kallberg, and S. Uppala, 1982: FGGE 4-dimensional data assimilation at ECMWF. *Bull. Amer. Meteor. Soc.*, **63**, 29–43.

Chen, T.-C., and Y.-H. Lee, 1984: A comparison of spectral energetic analyses using various FGGE III-b data. *Proc. of the First National Workshop on Scientific Results of the Global Weather Experiment*, Woods Hole, National Academy of Sciences, 222–242.

Daley, R., and K. Puri, 1980: Four-dimensional data assimilation and the slow manifold. *Mon. Wea. Rev.*, **108**, 85–99.

Fein, J. S., and J. P. Kuettner, 1980: Report of the summer Monex field phase. *Bull. Amer. Meteor. Soc.*, **51**, 461–474.

Fox-Rabinovich, M., and B. Gross, 1990: A forced diabatic initialization procedure for the GLA forecast and data assimilation system. Report of the WMO International Symposium on Assimilation of Observations in Meteorology and Oceanography. Clermont-Ferrand, France, 215–220.

He, H.-Y., J. W. McGinnis, Z.-S. Song, and M. Yanai, 1987: Onset of the Asian summer monsoon in 1979 and the effect of the Tibetan Plateau. *Mon. Wea. Rev.*, **115**, 1966–1995.

Hollingsworth, A., 1986: Objective analysis for numerical weather prediction. Short- and Medium-Range Weather Prediction Proc., Tokyo, WMO/IUGG NWP Symposium, 11–59.

——, A. C. Lorenc, M. S. Tracton, K. Arpe, G. Cats, S. Uppala, and P. Kallberg, 1985: The response of numerical weather prediction systems to FGGE II-b data, Part I: Analyses. *Quart. J. Roy. Meteor. Soc.*, **111**, 1–66.

Krishnamurti, T. N., 1985: Summer Monsoon Experiment—A review. *Mon. Wea. Rev.*, **113**, 1590–1626.

——, P. Ardanay, V. Ramanathan, and R. Pasch, 1981: On the onset vortex of the summer monsoon. *Mon. Wea. Rev.*, **109**, 344–363.

Kung, E. C., and H. Tanaka, 1983: Energetics analysis of the global circulation during the special observing periods of FGGE. *J. Atmos. Sci.*, **40**, 2575–2592.

Lau, K. M., and L. Peng, 1987: Origin of low frequency (intraseasonal) oscillations in the tropical atmosphere. Part I: The basic theory. *J. Atmos. Sci.*, **44**, 950–972.

Lau, N.-C., 1984a: Circulation statistics based on FGGE level III-b analyses produced by GFDL. NOAA Data Report ERL GFDL-5, 427 pp.

——, 1984b: A comparison of circulation statistics based on FGGE level III-b analyses produced by GFDL and ECMWF for the special observing periods. NOAA Data Report ERL GFDL-6, 237 pp.

Lorenc, A. C., 1984: The evolution of planetary scale 200 mb divergences during the FGGE year. *Quart. J. Roy. Meteor. Soc.*, **110**, 427–442.

McPherson, R. D., 1975: Progress, problems and prospects in meteorological data assimilation. *Bull. Amer. Meteor. Soc.*, **56**, 1154–1166.

Miyakoda, K., 1985: Assessment of results from different analysis schemes. *Proc. Results of the Global Weather Experiments and*

Their Implications for the World Weather Watch, Geneva, Switzerland, World Meteorological Organization.

——, R. F. Strickler, and T. Chludzinski, 1978: Initialization with the data assimilation method. *Tellus,* **30,** 32–54.

——, J. Ploshay, and W. Stern, 1983: Guide and caution on the GFDL/FGGE III-b data set. *GWE Newsletter,* **1,** 8–14.

Ploshay, J. J., R. White, and K. Miyakoda, 1983: FGGE level III-b daily global analyses. Part I, II, III, IV. NOAA Data Report ERL GFDL-1, 278 pp., 285 pp., 285 pp., 282 pp.

——, W. F. Stern, and K. Miyakoda, 1984: FGGE III-b data sets—reanalysis during SOP's at GFDL. GARP Special Report No. 44, Report of the seminar on progress in tropical meteorology as a result of the global weather experiment at Tallahassee, FL, October 1984, WMO/ICSU, pp. I-46–53.

——, ——, and ——, 1991: A summary report on FGGE re-analysis at GFDL. BMRC Research Report No. 27, "Data Assimilation Systems"; papers presented at the second BMRC modeling workshop, September 1990. Melbourne, Australia, 29–53.

Sikdar, D. N., and D. W. Martin, 1981: Satellite observed cloud fields in relation to the onset of southwest monsoon over India in 1979. Report of the international conference on early results of FGGE and large-scale aspects of its monsoon experiments at Tallahassee, FL, WMO/ICSU, 25–30.

Stern, W. F., and J. J. Ploshay, 1992: A scheme for continuous data assimilation. *Mon. Wea. Rev.,* **120,** 1417–1432.

——, ——, and K. Miyakoda, 1985: Continuous data assimilation at GFDL during FGGE. *Report at seminar/workshop on data systems and observing system experiments with particular emphasis on FGGE,* 1984, sponsored by ECMWF and WMO, Vol. 2, 125–156.

Tokioka, T., K. Yamazaki, A. Kitoh, and T. Ose, 1988: The equatorial 30–60 day oscillation and the Arakawa–Schubert penetrative cumulus parameterization. *J. Meteor. Soc. Japan,* **66,** 883–901.

Undén, P., 1989: Tropical data assimilation and analysis of divergence. *Mon. Wea. Rev.,* **117,** 2495–2517.